Title - Rescue of aberrant huntingtin palmitoylation ameliorates mutant huntingtin-induced toxicity

Authors – Fanny L. Lemarié[a], Nicholas S. Caron[a], Shaun S. Sanders[a,b], Mandi E. Schmidt[a], Yen T.N. Nguyen[a], Seunghyun Ko[a], Xiaohong Xu[d,e], Mahmoud A. Pouladi[a,d], Dale D.O. Martin[a,c], Michael R. Hayden[a]*

[a] Centre for Molecular Medicine and Therapeutics, BC Children's Hospital Research Institute, University of British Columbia, Vancouver, Canada

[b] Department of Molecular and Cellular Biology, University of Guelph, Guelph, Canada

[c] Department of Biology, University of Waterloo, Waterloo, Canada

[d] Translational Laboratory in Genetic Medicine, Department of Physiology, Yong Loo Lin School of Medicine, National University of Singapore, Singapore

[e] Department of Neurology and Stroke Center, The First Affiliated Hospital, Jinan University, Guangzhou, China

*To whom correspondence should be addressed (mrh@cmmt.ubc.ca)
Centre for Molecular Medicine and Therapeutics
BC Children's Hospital Research Institute
University of British Columbia
3025-950 West 28th Ave
Vancouver, BC Canada
V5Z 4H4
604-875-3535
mrh@cmmt.ubc.ca

Highlights:

- Palmitoylation of mHTT is reduced in multiple transgenic HD mouse models
- HTT palmitoylation decreases with increasing polyQ length in HD patient cells
- mHTT-lowering in mouse brains does not rescue aberrant palmitoylation
- mHTT palmitoylation in HD patient-derived cells can be rescued via APT inhibition
- Promoting palmitoylation reduces mHTT aggregation and cytotoxicity *in vitro*

Abstract: Huntington disease (HD) is a neurodegenerative disorder caused by a CAG expansion in the *HTT* gene that codes for an elongated polyglutamine tract in the huntingtin (HTT) protein. HTT is subject to multiple post-translational modifications (PTMs) that regulate its cellular function. Mutating specific PTM sites within mutant HTT (mHTT) in HD mouse models can modulate disease phenotypes, highlighting the key role of HTT PTMs in the pathogenesis of HD. These findings have led to increased interest in developing small molecules to modulate HTT PTMs in order to decrease mHTT toxicity. However, the therapeutic efficacy of pharmacological modulation of HTT PTMs in preclinical HD models remains largely unknown. HTT is palmitoylated at cysteine 214 by the huntingtin-interacting protein 14 (HIP14 or ZDHHC17) and 14-like (HIP14L or ZDHHC13) acyltransferases. Here, we assessed if HTT palmitoylation should be regarded as a therapeutic target to treat HD by (1) investigating palmitoylation dysregulation in rodent and human HD model systems, (2) measuring the impact of mHTT-lowering therapy on brain palmitoylation, and (3) evaluating if HTT palmitoylation can be pharmacologically modulate. We show that palmitoylation of mHTT and some HIP14/HIP14L-substrates is decreased early in multiple HD mouse models, and that aging further reduces HTT palmitoylation. Lowering mHTT in the brain of YAC128 mice is not sufficient to rescue aberrant palmitoylation. However, we demonstrate that mHTT palmitoylation can be normalized in COS-7 cells, in YAC128 cortico-striatal primary neurons and HD patient-derived lymphoblasts using an acyl-protein thioesterase (APT) inhibitor. Moreover, we show that modulating palmitoylation reduces mHTT aggregation and mHTT-induced cytotoxicity in COS-7 cells and YAC128 neurons.

52 **Keywords:** Palmitoylation; S-acylation; Huntingtin; Huntington Disease; ZDHHC17, Acyl-
53 Protein Thioesterase; Neuroprotection

54 **Abbreviations:** ABE, acyl-biotin exchange assay; APT, acyl-protein thioesterase; ASO,
55 antisense oligonucleotide; HD, Huntington disease; hiPSC, human induced pluripotent
56 stem cell; HIP14, huntingtin-interacting protein 14 (ZDHHC17); HIP14L, huntingtin-
57 interacting protein 14-like (ZDHHC13); HTT, huntingtin (human); Htt, huntingtin (mouse);
58 ICV, intracerebroventricular; LNA, locked nucleic acid; mHTT, mutant huntingtin; NEM,
59 N-ethylmaleimide; PalmB, palmostatin B; PAT, palmitoyl acyltransferase; PTM, post-
60 translational modification

61 **1. Introduction**

62 Huntington disease (HD) is an inherited neurodegenerative disorder characterized
63 by involuntary movements, behavioural changes and cognitive impairment. There are
64 currently no therapies available to influence its inexorable progression (Caron et al., 2018;
65 Evans et al., 2013; Fisher and Hayden, 2014; Myers, 2004). The genetic cause of HD is
66 an expanded CAG trinucleotide repeat (>35) in the *HTT* gene leading to an abnormally
67 long polyglutamine (polyQ) tract in the huntingtin (HTT) protein.

68 HTT interacts with numerous protein partners and is involved in many cellular processes,
69 including endocytosis, vesicle/organelle transport and recycling, autophagy, and DNA
70 transcription (Maiuri et al., 2017; Ochaba et al., 2014; Saudou and Humbert, 2016). HTT
71 is subject to numerous post-translational modifications (PTMs), including phosphorylation
72 (Aiken et al., 2009; Humbert et al., 2002; Schilling et al., 2006), acetylation (Jeong et al.,
73 2009), ubiquitination (Kalchman et al., 1996), SUMOylation (Steffan et al., 2004),
74 proteolysis (Graham et al., 2006), and fatty acylation (palmitoylation and myristoylation)
75 (Martin et al., 2018, 2014; Yanai et al., 2006). These PTMs regulate subcellular
76 localization, protein-protein interactions, aggregation and clearance which modulates the
77 toxicity of mutant HTT (mHTT) (Atwal et al., 2011, 2007; Cariulo et al., 2017; Caron et al.,
78 2013; Kratter et al., 2016; Lontay et al., 2020).

79 In the presence of the HD mutation, levels of several key PTMs are significantly altered
80 *in vitro* and *in vivo* (Cariulo et al., 2020, 2017; Warby et al., 2005). Introducing mutations
81 at specific PTM sites of mHTT has been shown to modulate disease phenotypes in
82 various HD models. Blocking proteolysis of mHTT at aspartic acid 586 (D586) prevents
83 striatal neurodegeneration in the YAC128 HD mouse model (Graham et al., 2006).

84 Blocking phosphorylation at serine residues 13/16 or 421 (S13/16A, S421A) in the
85 BACHD mouse model and HD human induced pluripotent stem cell (hiPSC)-derived
86 neural cells exacerbates disease phenotypes. In contrast, mimicking phosphorylation at
87 these residues (S13/16D, S421D) prevents neurodegeneration in these same models (Gu
88 et al., 2009; Kratter et al., 2016; Xu et al., 2020). These findings highlight the key role of
89 HTT PTMs in the pathogenesis of HD and have stimulated interest in the development of
90 drugs to modulate HTT PTMs in order to decrease mHTT levels and toxicity. To date,
91 most research has focused on normalizing HTT phosphorylation at S13 and S16, and
92 preventing mHTT proteolysis (Aharony et al., 2015; Atwal et al., 2011; Bowie et al., 2018).

93 Palmitoylation refers to the addition of a palmitic acid (C16:0) onto a cysteine
94 residue via a thioester bond. This process is catalyzed by a family of palmitoyl
95 acyltransferases (PATs). Palmitoylation increases the hydrophobicity of proteins, and
96 therefore plays a key role in protein trafficking, stability, membrane association and
97 protein-protein interactions (Fukata and Fukata, 2010). It is the most common protein-
98 lipid modification in the brain (Smotrys and Linder, 2004). Importantly, it is reversible and
99 allows for dynamic regulation of protein functions at the synapse, thus playing an
100 important role in neurodevelopmental processes and in neuronal survival (Globa and
101 Bamji, 2017; Hubalkova et al., 2021; Matt et al., 2019; Mukai et al., 2008). Disruption of
102 protein palmitoylation has been implicated in the pathogenesis of several neurological
103 disorders, including Alzheimer's disease, schizophrenia and intellectual disability (Cho
104 and Park, 2016; Sanders et al., 2015b).

105 We first described that HTT is palmitoylated at cysteine 214 (C214), a reaction catalyzed
106 by the palmitoyl acyltransferases ZDHHC17 and ZDHHC13, also known as huntingtin-

107 interacting protein 14 and 14-like (HIP14 and HIP14L) (Yanai et al., 2006). In the presence
108 of the HD mutation, mHTT was found to be hypo-palmitoylated in the brain of the YAC128
109 HD mouse model (Yanai et al., 2006). Transient expression of mHTT carrying a
110 palmitoylation-resistant mutation (C214 to serine, C214S) in immortalized cell lines and
111 primary neurons led to increased aggregates and nuclear inclusion formation, increased
112 cell death and increased susceptibility to excitotoxicity (Yanai et al., 2006).
113 Autopalmitoylation of HIP14 and HIP14L, and palmitoylation of many of their synaptic
114 substrates were also downregulated in the YAC128 HD mouse brains or in the brains of
115 mice lacking one *Htt* allele (*Htt*$^{+/-}$) (Huang et al., 2011; Singaraja et al., 2011). Moreover,
116 mouse models deficient in either HIP14 (*Hip14*$^{-/-}$) or HIP14L (*Hip14l*$^{-/-}$) develop
117 neuropathological deficits that are reminiscent of HD (Sutton et al., 2013), and loss of
118 both *Hip14* and *Hip14l* leads to embryonic lethality (Sanders et al., 2016, 2015a).
119 Collectively, these findings link defects in fatty acylation with neuronal dysfunction and
120 neurodegeneration in HD. However, the effect of palmitoylation on HTT function and the
121 role that loss of HTT palmitoylation plays in the pathogenesis of HD are still not fully
122 elucidated.

123 In this study, we investigate whether palmitoylation is dysregulated in HD mouse
124 models and human HD samples. We also evaluate whether pharmacological modulation
125 of mHTT palmitoylation represents a potential therapeutic target for the treatment of HD.

126 **2. Materials and methods**

127 **2.1. Materials**

128 **2.1.1. Reagents and chemicals**

129 **Table 1** lists the reagents and chemicals used for this study along with the application,
130 manufacturer and catalogue number.

131 **2.1.2. Antibodies**

132 **Table 2** displays the list of antibodies used along with the application, concentrations and
133 experimental conditions.

134 **2.1.3. Experimental models**

135 **HD mouse lines** - Heterozygous YAC128 (line 53), homozygous YAC128 (line 55),
136 homozygous YAC18 (line 60), BACHD, humanized Hu18/18 and Hu97/18, humanized
137 Hu21/21 and Hu128/21 mice were maintained on the FVB/N background. The description
138 of the HD mouse lines used is displayed in **Table 3**. The YAC128 model expresses two
139 mouse Htt alleles and the full length human mHTT transgene (Slow et al., 2003). The
140 BACHD model expresses two mouse Htt alleles and the full length human mHTT
141 transgene (Gray et al., 2008). The two humanized Hu97/18 and Hu128/21 models
142 express only full length human WT and mHTT transgenes and no mouse Htt complement
143 (Southwell et al., 2017, 2013). Experiments were performed according to protocols
144 approved by the University of British Columbia Animal Care Committee (experimental
145 protocol 2016/2020 #A20-0107, breeding protocol #A20-0233). Homozygous YAC128
146 and YAC18 mice were used for the neuronal culture, to improve culture health by avoiding
147 an overnight genotyping step. For all cohorts, approximately equal numbers of male and

148 female mice were used. All mice were sacrificed using CO_2 asphyxiation in accordance
149 with UBC SOP #I012.

150 **Cell line culture** – Control and HD patient-derived lymphoblastoid cell lines (**Table 4**)
151 were obtained from the NIGMS Human Genetic Cell Repository at the Coriell Institute for
152 Medical Research. All cell lines were maintained in RPMI 1640 medium containing 10%
153 FBS, 2 mM GlutaMAX, 10 units/mL of penicillin and 10 µg/mL of streptomycin. Cells were
154 grown in T-25 flasks incubated in an upright position with vented caps at 37°C and 5%
155 CO_2. Cell density was kept between 2.10^5 and 5.10^5 cells/mL of media.

156 COS-7 cells were grown in DMEM medium supplemented with 10% FBS, 1 mM sodium
157 pyruvate, 2 mM GlutaMAX, 10 units/mL of penicillin and 10 µg/mL of streptomycin. Cells
158 were grown in 10-cm plates at 37°C and 5% CO_2, and were split using a 0.25% trypsin
159 solution (1:10 dilution) when cells were ~90% confluent by microscopy.

160 Human pluripotent stem cells (hPSCs) lines listed in **Table 5** were cultured on Matrigel-
161 coated plates in mTeSR-1 complete medium supplemented with 10 units/mL of penicillin
162 and 10 µg/mL of streptomycin at 37°C and 5% CO_2, and were split with ReLeSR.

163 **Neuronal culture** - Timed pregnancies were set up by mating homozygous YAC18 (line
164 60) or YAC128 (line 55) mice. At E16.5, embryos were removed from pregnant females.
165 Cortical and striatal tissues attached were dissected in ice-cold HBSS, gently dissociated
166 with a P1000 pipette (×2-3 times) and briefly spun. Tissues were digested in 0.05%
167 trypsin-EDTA for 8 min at 37°C until addition of 10% FBS in neurobasal (NB) medium, as
168 previously described (Schmidt et al., 2020). Cells were centrifuged, further dissociated by
169 mechanical trituration in NB medium (supplemented with B27, GlutaMAX, penicillin and
170 streptomycin) and DNase (0.08 mg/mL). Neurons were plated in 6-well Nunclon Delta

171 surface plates at a density of 1.10^6 cells/well in 2 mL of complete NB medium. Prior to
172 plating, 6-well plates were coated with sterile-filtered 50 µg/mL of poly-D-lysine
173 hydrobromide for 2 h at room temperature and washed four times with sterile water. All
174 cultures were regularly supplemented with fresh complete NB medium (20% well volume).

175 **2.2. Methods**

176 **2.2.1. Plasmid transfection**

177 COS-7 cells were seeded in 6-well or 96-well plates overnight at 37°C and 5% CO_2. The
178 next day, cells were transfected with cDNA plasmid constructs encoding for 15Q and
179 mutant 128Q N-terminus HTT_{1-548} (N548), HTT_{1-1212} (N1212) and full-length HTT_{1-3144}
180 (HTT), or 17Q and 138Q HTT_{1-588}-YFP (N588) using X-tremeGENE 9 DNA transfection
181 reagent (ratio 3:1, reagent (µL): DNA (µg)). Cells were treated or harvested 18 to 24h
182 post-transfection.

183 **2.2.2. Acyl-protein thioesterase (APT) inhibition with palmostatin B**

184 ***Inhibition of APTs in immortalized cell lines***

185 At 18-24h post-transfection, COS-7 cells were deprived of lipid for 1 h in DMEM (without
186 methionine or cysteine) supplemented with 5% Charcoal stripped FBS, subsequently
187 treated with DMSO or 15 µM Palmostatin B (PalmB) (diluted in DMSO at 1000X on
188 InSolution) while concurrently metabolically labelled with 100 µM alkyne-palmitate for 6h.
189 Bio-orthogonal click chemistry of alkyne-palmitate was performed as subsequently
190 described in section §2.2.4.

191 ***Inhibition of APTs in primary neurons***

192 Primary neurons from cortex and striatum of E16.5 mouse embryos (homozygous YAC18
193 and YAC128 mouse lines) were cultured as previously described in section §2.1.3. At

194 DIV10, neuronal cultures were treated with DMSO or with 15 μM PalmB (InSolution) for
195 6h. The IP-ABE assay was performed on neuronal lysates as described in section §2.2.4.

196 ***Inhibition of APTs in control and HD patient-derived lymphoblastoid lines***

197 Lymphoblasts were cultured as previously described in section §2.1.3. Cells were seeded
198 at a density of 600,000 cells/2 mL/well in 6 well plates. The next day, cells were treated
199 with DMSO or 10 μM PalmB for 4h. The IP-ABE assay was performed on lymphoblasts
200 as described in section §2.2.4.

201 **2.2.3. Intracerebroventricular HTT antisense oligonucleotide infusion**

202 A fully phosphorothioate modified gapmer ASO with 5' locked nucleic acid (LNA)
203 modifications in each wing, matching a sequence in intron 22 of the *HTT* gene (5'-
204 TAATACGTAAGTGTCACAA-3', custom synthesized by Qiagen) was delivered by
205 intracerebroventricular (ICV) injection as previously described (Southwell et al., 2015).
206 Five-month-old YAC128 (line 53) mice were anesthetized using 3% isoflurane and
207 secured on a stereotaxic frame. Mice were given pre-operative subcutaneous
208 buprenorphine (0.1 mg/kg) and 0.25% bupivacaine at the site of incision. A midline
209 incision was made in the scalp to expose the skull. Then, a 50 μL Hamilton syringe with
210 a 26-gauge needle was oriented to the bregma and moved 0.3 mm anterior, 1 mm lateral,
211 and 3 mm ventral. An injection volume of 10 μL was delivered into the lateral ventricle at
212 a rate of 5 μL/min. Mice were either injected with 50 μg ASO in sterile PBS (n=7) or PBS
213 only (n=6). The needle was left in place for 2 min after injection, before being slowly
214 retracted. The scalp was closed with sutures and Vetbond tissue adhesive. Animals were
215 then placed in a recovery cage with a heating pad, hydrogel, and food on the cage floor.
216 Mice were given post-operative buprenorphine as needed and monitored for 72h.

217 **2.2.4. Palmitoylation assays**

218 ***Acyl-biotin exchange assay on immunoprecipitated proteins (IP-ABE)***

219 **Mouse brain** – IP-ABE assays were performed on whole or half frozen brain samples
220 from YAC128 (line 53) and WT littermate controls, BACHD and WT littermate controls,
221 Hu97/18 and Hu18/18, Hu128/21 and Hu21/21, as previously described (Drisdel and
222 Green, 2004; Huang et al., 2009). Briefly, brains were harvested and immediately snap-
223 frozen in liquid N_2 and stored at -80°C until being processed. Frozen brains were
224 homogenized on ice in lysis buffer (150 mM NaCl, 50 mM Tris, 5 mM EDTA, 0.1% SDS,
225 1% triton X-100, pH 7.4) with 100 mM NEM (4 mL lysis buffer/brain hemisphere).
226 Homogenates were sonicated for 15 sec at 30% power to shear DNA and the insoluble
227 material was removed by centrifugation at 20,000 × g for 15 min at +4°C. Protein
228 concentrations in lysates were assessed by DC protein assay. HTT, PSD95, and GAD65
229 were immunoprecipitated (IP) from brain lysates (300 µL) by overnight incubation with
230 Protein G Dynabeads or PureProteome protein A/G, and appropriate antibodies for
231 immunoprecipitation (**Table 2**). Beads were then washed and split into two and treated
232 either with neutral pH hydroxylamine (HAM+) in lysis buffer or just lysis buffer (HAM-) for
233 2h for HTT and 1h for the other three proteins at room temperature. Following HAM
234 treatment, beads were washed and treated with 2.5 µM EZ-Link BMCC-Biotin in pH 6.2
235 lysis buffer for 1h at 4°C. At the end of the BMCC-Biotin treatment, beads were washed
236 and heated at 70°C for 10 min with NuPAGE LDS sample buffer and 100 mM DTT to
237 elute proteins.

238 **Control and HD-patient derived lymphoblastoid and hiPSC lines** – Lymphoblastoid
239 aggregates in suspension in the media were dissociated by trituration and centrifuged for

240 5 min at 500 × g at room temperature. HiPSCs were washed with DMEM/F12, lifted from
241 plated using ReLeSR and spun at 500 × g for 5 min at +4°C. Supernatant was discarded
242 and cell pellets were frozen until being processed, as previously described for mouse
243 brain samples. HTT was immunoprecipitated from cell lysates by overnight incubation
244 with Protein G Dynabeads and HTT (MAB2166) antibodies (approx. 250 µg protein and
245 2 µL MAB2166 for 20 µL beads).

246 ***Bio-orthogonal labelling assay using alkyne-palmitate***

247 **Immortalized cell lines** - cells transiently transfected with cDNA HTT constructs were
248 deprived of lipid during 1 h incubation in DMEM supplemented with 5% charcoal stripped
249 FBS 18h post-transfection and subsequently metabolically labelled with 100 µM alkyne-
250 palmitate for 6 h. Cells were lifted from plates in PBS using cell scrapers, pelleted by
251 centrifugation (500 × g, 5 min, +4°C) and subsequently lysed in RIPA (150 mM $NaCl_2$, 5
252 mM M EDTA, 50 mM Tris, 1% NP-40, 0.5% sodium deoxycholate, 0.1% SDS in dH_2O,
253 complete protease inhibitors cocktails) or SDP lysis (50 mM Tris pH 8.0, 150 mM NaCl,
254 1% Igepal, 40 mM NaF, 1 mM PMSF, 2 mM sodium vanadate, complete protease
255 inhibitors cocktails) buffer for 10 min on ice, 5 min at 4°C on rotator and were centrifuged
256 (16,000 × g, 10 min, 4°C). Bio-orthogonal click chemistry of alkyne-palmitate was
257 performed, as previously described (Yap et al., 2010) on cell lysates immunoprecipitated
258 with anti-HTT antibodies (BKP1 or MAB2166). HTT immunoprecipitates were adjusted to
259 1% SDS and incubated with 100 mM TBTA, 1 mM $CuSO_4$, 1 mM TCEP and 100 mM
260 azido-biotin at +37°C in darkness for 1 h.

261 **2.2.5. Western blot analysis**

262 Brain, COS-7 and HD patient-derived hiPSC and lymphoblastoid supernatants from HTT
263 assays were run on NuPAGE™ 3-8% Tris-Acetate gradient protein gels in Tris-Acetate
264 SDS Running Buffer (50 mM Tricine, 50 mM Tris Base, 0.1% SDS, pH 8.24) or
265 homemade 8% low bis acrylamide (1:200 bis-acrylamide:acrylamide) gels in SDS-Tris-
266 glycine running buffer (25 mM Tris base, 190 mM glycine, 3.5 mM SDS) (Carroll et al.,
267 2011) to resolve full length HTT alleles with small ΔQs. Brain lysates from the other
268 proteins (SNAP25, PSD95 and GAD65) were run on homemade tris-glycine gels (7-12%)
269 in SDS-Tris-glycine running buffer. Protein were transferred to 0.45 µm nitrocellulose.
270 Membranes were blocked with 5% milk in Phosphate-Buffered Saline (PBS) or 3-5% BSA
271 in Tris-Buffered Saline (TBS) supplemented with 0.1-0.5% Tween-20 (T). Primary
272 antibody dilutions of HTT (D7F7 or MAB2166), SNAP25 polyclonal, PSD95 monoclonal,
273 and GAD65 polyclonal in 3-5% BSA PBST or TBST were applied to the immunoblots at
274 room temperature for 1h or overnight at +4°C (**Table 2**). Membranes were washed 4 × 5
275 min in PBST or TBST. The appropriate secondary antibodies and Alexa Fluor 680
276 conjugated streptavidin were applied in 3-5% BSA PBST or TBST for 1 to 2h at room
277 temperature. Membranes were washed 4 × 5 min in PBST or TBST and imaged using
278 the LI-COR Odyssey Infrared Imaging System (Li-Cor Biosciences). Densitometry was
279 quantified using the LiCor Image Studio Lite software and median signal intensity
280 following background subtraction was used for analysis. Palmitoylation was analyzed as
281 a ratio of HAM+ palmitoylation signal to total immunoprecipitated protein signal and
282 normalized to the control.

283 **2.2.6. Aggregation and cytotoxicity assays**

284 ***Filter retardation assay***

285 Protein aggregation of insoluble HTT_{1-588}-YFP transiently expressed in COS-7 cells was
286 measured using the filter-trap retardation assay, as previously described (Dale D. O.
287 Martin et al., 2018; Wanker et al., 1999). After 72 h of transfection, COS-7 cells expressing
288 the indicated HTT_{1-588}-YFP constructs and treated with 15 µM PalmB for 48h were lysed
289 in lysis buffer (50 mM Tris pH 8.8, 100 mM NaCl, 5 mM $MgCl_2$, 0.5% Igepal CA630, 1 mM
290 EDTA with 1X cOmplete protease inhibitor cocktail and 25 unit/mL benzonase fresh)
291 (~150 µL/cell pellet) for 30 min on ice without vortexing or spinning (only pipetting to
292 homogenize). Protein concentrations in lysates were assessed by DC protein assay and
293 adjusted to 1 µg/µL in a total volume of 50 µL. Samples (50 µg of proteins) were denatured
294 in a 1:1 volume of denaturation buffer (2% SDS and 50 mM DTT) at 98°C for 10 min.
295 Denatured samples were loaded in duplicate over a 0.2 µm cellulose acetate (OE66)
296 membrane positioned in the filter retardation apparatus (Whatman, The Convertible
297 filtration manifold system cat. Series 1055). The membrane was washed with a 0.2% SDS
298 solution once prior to loading the samples, and twice after (100 µL/wash). The membrane
299 was blocked in 3% BSA TBST (0.1% Tween 20) for an hour and probed by standard
300 immunoblotting analysis with primary mouse anti-HTT (MAB2166) and rabbit anti-GFP
301 antibodies, followed by secondary antibodies and detection using the LI-COR Odyssey
302 immunoblotting system. The quantity of aggregates retained on the filter expressed was
303 measured with Image Studio Lite and calculated relatively to the PBS control group
304 (arbitrarily set at 1) and technical replicates were averaged.

305 ***LDH activity cytotoxicity assay***

306 Cytotoxicity was assessed in COS-7 transiently expressing human HTT or YAC128
307 neurons after 6 and 24h of PalmB treatment, using the CYQUANT LDH cytotoxicity assay
308 kit, as per the manufacturer's guidelines. Lactate dehydrogenase (LDH) is a well-defined
309 and reliable indicator of cytotoxicity. Extracellular LDH was here quantified by a coupled
310 enzymatic reaction in which LDH catalyzes the conversion of lactate to pyruvate via NAD+
311 reduction to NADH. This can be measured by using an excitation of 560 nm and an
312 emission of 590 nm. A cell density of 10,000 cells/well was chosen after experimental
313 optimization. Fluorescence was read on an EnSpire 2300 Multilabel plate reader from
314 PerkinElmer using the EnSpire manager software. Cytotoxicity (in %) was calculated
315 using the formula:

316 $$\%\,Cytotoxicity = \left(\frac{Compound\ treated\ LDH\ activity^{1} - Spontaneous\ LDH\ activity^{2}}{Maximum\ LDH\ activity^{3} - Spontaneous\ LDH\ activity^{2}}\right) \times 100$$

317 [1] fluorescence in transfected COS-7 cells or YAC128 neurons treated with PalmB (x%),
318 [2] fluorescence in untransfected COS-7 cells untreated or YAC128 neurons treated with DMSO (0%),
319 [3] fluorescence in untransfected COS-7 cells or YAC128 neurons treated with 10X lysis buffer (100%).

320 **2.2.7. Statistical Analysis**

321 GraphPad Prism 9 was used for all statistical analysis and graph preparation. Figures
322 were generated in Adobe Illustrator 2020. All data are presented as mean ± SEM.
323 Biological replicates (n) are displayed on each graph, or indicated in the captions.
324 Student's t-test or 1- or 2-way ANOVA statistical tests with post-hoc analysis (Tukey,
325 Dunnett, Sidak or Bonferroni) were used for all experiments. In some cases, t-tests were
326 performed between specific groups after an ANOVA test when a planned comparison
327 was established during the experimental design process. Significance for these tests is
328 noted with the "#" symbol instead of "*".

329 **3. Results**

330 **3.1. Palmitoylation levels of HTT and HIP14/HIP14L substrates are decreased in the**
331 **BACHD and in two humanized HD mouse models**

332 We first wanted to assess in a low throughput, high confidence manner how the
333 presence of mHTT impacts protein palmitoylation in multiple mouse models of HD,
334 including BACHD, YAC128, Hu97/18 and Hu128/21 (**Table 3**). We therefore compared
335 levels of palmitoylation of HTT as well as HIP14 and/or HIP14L substrates: 25 kDa
336 synaptosomal-associated protein (SNAP25), 95 kDa post-synaptic density protein
337 (PSD95), and 65 kDa glutamate decarboxylase (GAD65) in the brains of 6-month-old HD
338 mouse lines and their respective control line (**Figure 1**).

339 In the BACHD model (**Figure 1.B**), the palmitoylation level of mHTT Q97 was
340 significantly lower (70%) than palmitoylation of mouse Htt Q7 in the WT or HD brains (1-
341 way ANOVA (1WA): $p<0.0001$; Tukey's post-test (Tk): $p<0.0001$ for Q97 vs. Q7 in WT or
342 HD brains). In the humanized Hu97/18 and Hu18/18 brains (**Figure 1.C** - 1WA:
343 $p=0.0002$), the palmitoylation level of mHTT Q97 was significantly lower than wtHTT Q18
344 in the Hu97/18 (50%; Tk: $p=0.0002$) and Hu18/18 (40%; Tk: $p=0.0023$) brains. In the
345 Hu128/21 and Hu21/21 brains (**Figure 1.D** - 1WA: $p<0.0001$), the palmitoylation level of
346 mHTT Q128 was significantly lower than wtHTT Q21 in the Hu128/21 (20%; Tk:
347 $p=0.0004$) and Hu21/21 (30%; Tk: <0.0001) brains. In the YAC128 model (**Figure 1.A** -
348 1WA: $p<0.0001$), palmitoylation of mHTT Q128 was significantly decreased compared to
349 endogenous mouse Htt Q7 expressed in the YAC128 brain (60%; Tk: $p<0.0001$) and in
350 the WT littermate control brain (70%; Tk: $p<0.0001$), consistent with the 80% decrease of
351 mHTT Q128 compared to wtHTT Q18 in the YAC18 brain (Yanai et al., 2006).

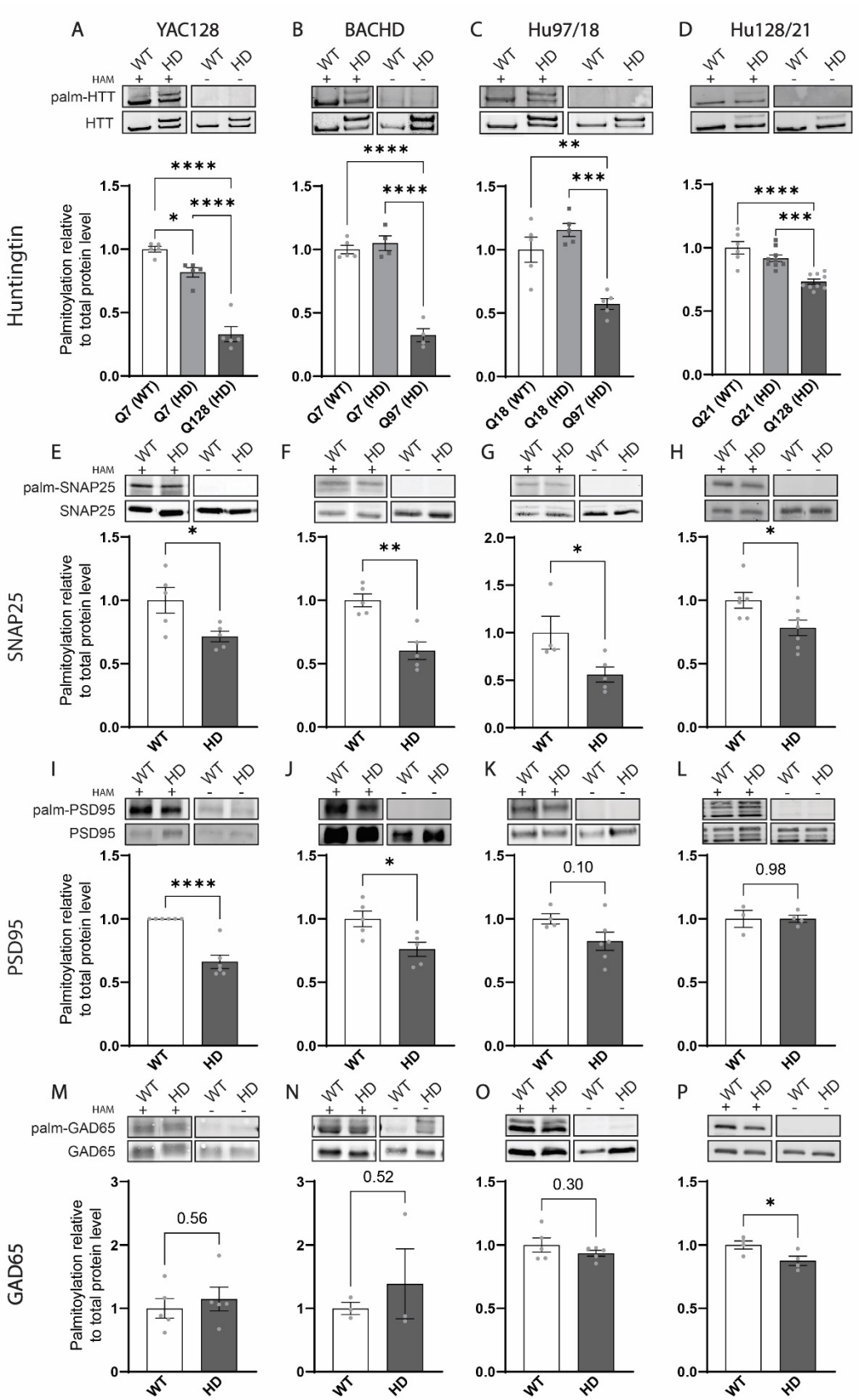
A
YAC128
B
BACHD
C
Hu97/18
D
Hu128/21
WT
HD
HAM
palm-HTT
HTT
Huntingtin
Palmitoylation relative to total protein level
Q7 (WT)
Q7 (HD)
Q128 (HD)
Q97 (HD)
Q18 (WT)
Q18 (HD)
Q21 (WT)
Q21 (HD)
E
F
G
H
palm-SNAP25
SNAP25
SNAP25
I
J
K
L
palm-PSD95
PSD95
PSD95
0.10
0.98
M
N
O
P
palm-GAD65
GAD65
GAD65
0.56
0.52
0.30

352

353 **<u>Figure 1</u> – Palmitoylation levels of mutant HTT, SNAP25, PSD95 and GAD65 are**
354 **reduced in the BACHD, and humanized Hu97/18 and Hu128/21 mouse models of**
355 **HD.**

356 Brain lysates from 6-month-old YAC128 and littermate controls (WT), BACHD and WT,
357 humanized Hu97/18 and Hu18/18, Hu128/21 and Hu21/21 mice were subjected to the
358 IP-ABE assay. The palmitoylation signal (HAM+) is shown in the top panels for each
359 mouse line and protein, and the total protein immunoprecipitated is presented in the
360 corresponding bottom panel. The negative control (HAM-) treatment is displayed on the
361 right of each set of blots. In the huntingtin (HTT) blots (**A-D**), the lower band corresponds
362 to Htt or wtHTT, and the upper band to mHTT. The palmitoylation levels for HTT (**A-D**),
363 SNAP25 (**E-H**), PSD95 (**I-L**) and GAD65 (**M-P**) were calculated as a ratio of palmitoylation
364 over total protein signal. Mutant HTT was quantified separately from Htt or wtHTT and is
365 represented by dark grey bars on the graphs, while Htt/wtHTT from the same HD brain is
366 in light grey.

367 <u>Statistical analysis</u>: 1-way ANOVA: (**A**) YAC128 and (**B**) BACHD, p<0.0001; (**C**) Hu97/18,
368 p=0.0002; (**D**) Hu128/21, p=0.0013. Stars indicate Tukey's multiple comparisons test
369 results. Student's T-test: (**E-P**) results are indicated by stars or p-values on the graphs.

370 HIP14 (ZDHHC17) and HIP14L (ZDHHC13) show substrate specificity for
371 neuronal proteins, including SNAP25, PSD95, and GAD65 (Huang et al., 2004), which all
372 play important roles in synaptic transmission. We therefore assessed palmitoylation levels
373 of these proteins in all four HD mouse models. SNAP25 palmitoylation was decreased by
374 30% in the YAC128 brain (**Figure 1.E** - Student's test, p=0.031), 40% in the BACHD brain
375 (**Figure 1.F** - p=0.0017), 45% in the Hu97/18 brain (**Figure 1.G** - p=0.041) and 20% in
376 the Hu128/21 brain (**Figure 1.H** - p=0.029) compared to their respective controls. PSD95
377 palmitoylation was also significantly decreased in the YAC128 brain (**Figure 1.I** - 35%;
378 p<0.0001) and the BACHD brain (**Figure 1.J** - 25%; p=0.020) compared to WT littermate
379 control brains. PSD95 palmitoylation showed a trend towards being reduced in the
380 Hu97/18 brain (**Figure 1.K** - 23%; p=0.10), but was unchanged in the Hu128/21 brain
381 (**Figure 1.L** - p=0.98) compared to controls. In contrast, palmitoylation of GAD65 was
382 unchanged in the YAC128, BACHD and Hu97/18 mouse models (**Figure 1.M-N-O**), but

383 was decreased by 15% in the brain of Hu128/21 (**Figure 1.P** - p=0.043) compared to the
384 Hu21/21 mice.

385 Our data shows that palmitoylation levels of HTT and various HIP14/14L
386 substrates are reproducibly reduced in all four HD mouse models. The absence of
387 endogenous Htt in the humanized HD brain does not exacerbate protein palmitoylation
388 dysregulation but may reveal subtle differences in palmitoylation dysregulation for GAD65
389 and PSD95.

390 **3.2. Palmitoylation of mutant HTT is decreased early in the brain of the humanized**
391 **HD mouse model, Hu128/21**

392 Our next goal was to investigate if aging affects palmitoylation of HTT in the brain
393 of humanized Hu128/21 HD mice. Palmitoylation of wtHTT and mHTT in the brain of
394 Hu21/21 and Hu128/21 mice at 1, 3, 6 and 12 months of age was measured using the IP-
395 ABE assay (**Figure 2.A-B-C-D**). At all the ages investigated, mHTT palmitoylation was
396 significantly lower than the palmitoylation level of wtHTT expressed in the control brain
397 (30-40%) or the HD brain (20-40%) (1WA: $p<0.01$ at 1 and 3 months, $p<0.001$ at 6 and
398 12 months). Notably, the decreased palmitoylation of mHTT was most pronounced at 6
399 and 12 months of age (**Figure 2.C and D**).

400 We then directly compared palmitoylation levels of wt and mHTT at different ages
401 in Hu21/21 (**Figure 2.E**) or Hu128/21 brain lysates (**Figure 2.F**) and found that
402 palmitoylation levels of wtHTT (1WA, p=0.0022) and mHTT (2-way ANOVA (2WA),
403 $p<0.0001$) significantly declined with age, reaching a 30% decrease at 12 months
404 compared to wt and mHTT palmitoylation levels at 1 month. This decline of HTT

405 palmitoylation with age was observed for both wt and mHTT, independent of the presence
406 of the HD mutation in the mouse brain. Taken together, our data demonstrates that
407 palmitoylation of HTT is decreased with age and further decreased in the presence of the
408 HD mutation as early as 1 month of age in the humanized Hu128/21 HD mouse model.

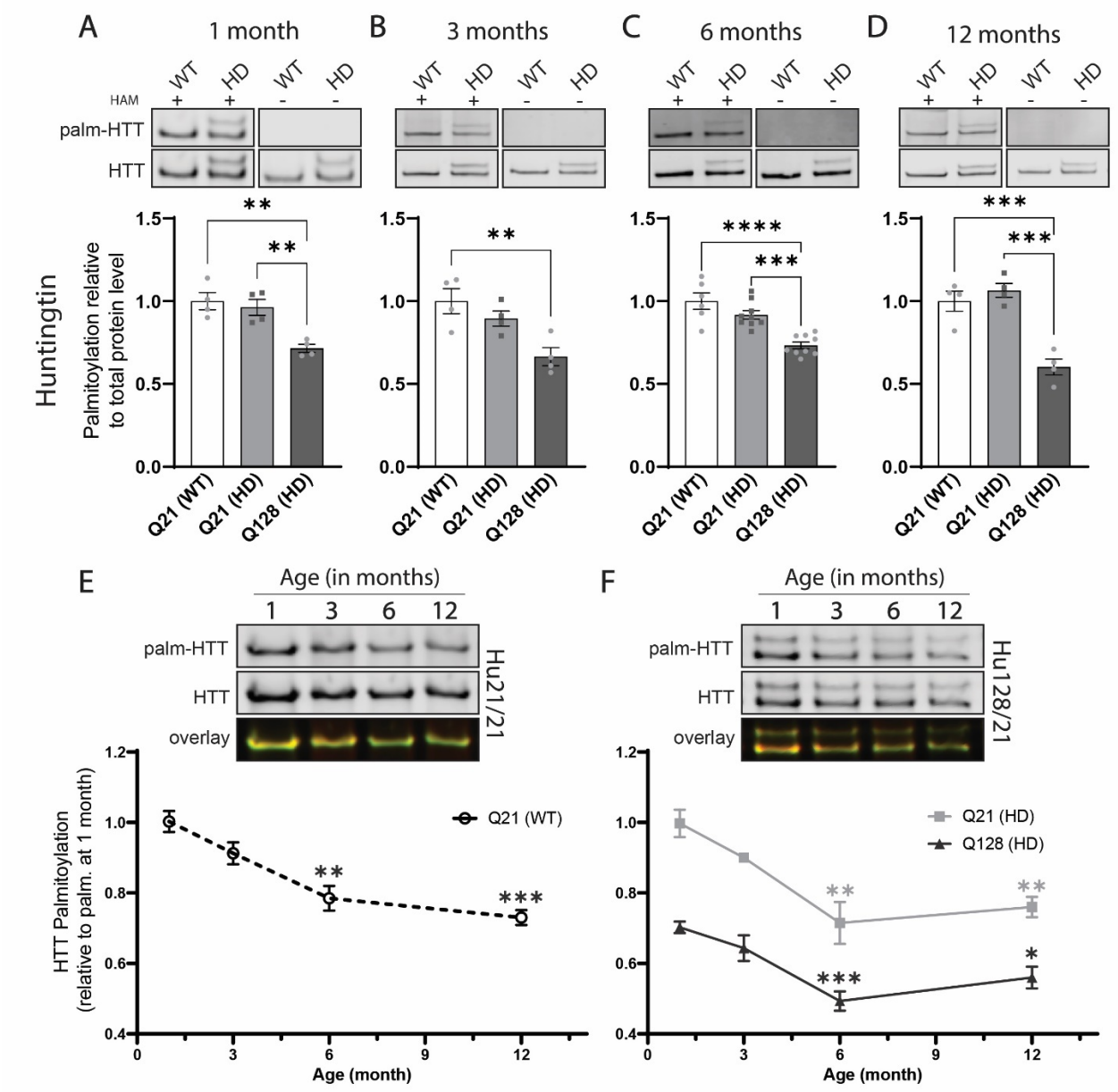

409

410 **<u>Figure 2</u> - Palmitoylation of mutant HTT is decreased early in the brain of the**
411 **humanized Hu128/21 mouse model of HD.**

412 HTT palmitoylation at (**A**) 1, (**B**) 3, (**C**) 6 and (**D**) 12 months measured using the IP-ABE
413 assay in brain lysates from Hu21/21 (WT) and Hu128/21 (HD) mice. The palmitoylation
414 signal (HAM+) is shown in the top panels for each time point, and the total protein
415 immunoprecipitated is presented in the corresponding bottom panel. The negative control
416 (HAM-) treatment is displayed on the right of each set of blots. Wildtype wtHTT (Q21) is
417 the lower band and mHTT (Q128) the upper one. The quantification of 4-9 mice of each
418 genotype is shown and was calculated as a ratio of HTT palmitoylation signal over total
419 HTT and expressed relatively to wtHTT in the Hu21/21 brain. In the Hu128/21 brain,
420 mHTT was quantified separately from wtHTT and is represented by dark grey bars while
421 wtHTT from the same HD mice is represented by light bars.

422 Effect of aging (1, 3, 6 and 12 months) on the palmitoylation levels of wt and mHTT in
423 lysates from Hu21/21 (**E**) and Hu128/21 (**F**) brains. Total brain lysates at different ages
424 were subjected to the IP-ABE assay and run on the same gel for each genotype (n=3-4).
425 Overlay of both channel (palm-HTT in red and total HTT in green) are displayed in the
426 bottom panels. Palmitoylation levels of wt and mHTT brain are expressed relatively to
427 wtHTT palmitoylation at 1 month.

428 Statistical analysis: 1-way ANOVA: (**A**) p=0.0022; (**B**) p=0.0094; (**C**) p<0.0001; (**D**)
429 p=0.0002. Stars indicate Tukey's multiple comparisons test results. (**E**) 1-way ANOVA:
430 p=0.0022. Stars indicate Dunnett's test results compared to 1 month. (**F**) 2-way ANOVA:
431 interaction, p=0.58; age and allele effect, p<0.0001. Stars indicate Dunnett's test results
432 compared to wtHTT (Q21) or mHTT (Q128) at 1 month, and therefore only show the effect
433 of age and not the effect of the HD mutation.

434 3.3. HTT palmitoylation levels in human lymphoblasts decrease with increasing 435 polyQ tract length

436 To further characterize palmitoylation dysregulation in HD, we assessed the impact
437 of the polyQ tract length on HTT palmitoylation in control and HD patient lymphoblasts
438 (**Figure 3.A, Table 4**). In the control lymphoblasts, wtHTT polyQ tracts were
439 approximately 17Qs in length. In the HD lymphoblasts, we stratified samples into two sub-
440 groups where mHTT polyQ tract lengths were either approximately 44Q or above 59Q.
441 The wtHTT protein in the HD lines had polyQ tracts with 17Qs.

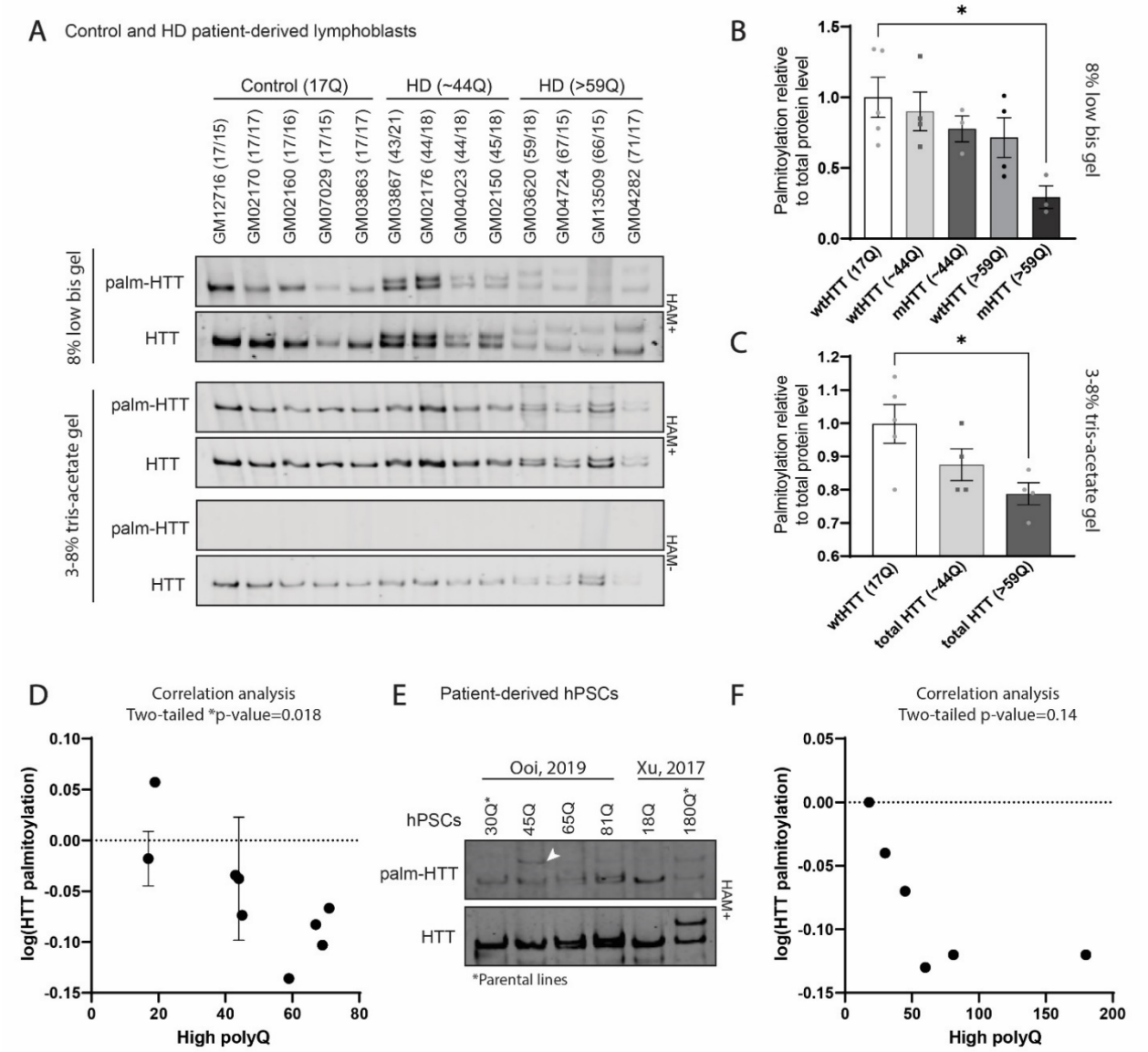

<u>Figure 3</u> - HTT palmitoylation levels decrease with increasing polyQ tract length in human lymphoblasts.

(**A**) HTT (wt and mHTT) palmitoylation levels in control and HD-patient derived lymphoblasts with increasing polyQ tract length (17 to 71). Proteins were resolved using 8% low bis or 3-8% tris-acetate gels. Palmitoylation is shown in the top panels (HAM+), and the total protein immunoprecipitated with anti-HTT (D7F7) antibodies are shown in the corresponding bottom panels. The negative control (HAM-) is shown below. Each lane corresponds to a lymphoblastoid line from a control or HD patients, and represents a biological replicate (n=4-5 for each group).

(**B**) Quantification of wt or mHTT palmitoylation levels in control and HD lymphoblasts in the control (17Q), HD (~44Q) and HD (>59Q) groups after protein separation using 8% low bis gel. The quantification is shown and is calculated as a ratio of HTT palmitoylation

signal over total HTT protein and expressed relatively to wtHTT palmitoylation in the control group (17Q).

(**C**) Quantification of HTT (wt and mHTT together) global palmitoylation levels measured in control (17Q), HD (~44Q) and HD (>59Q) lymphoblasts. Global palmitoylation levels of HTT was calculated as a ratio of wt and mHTT palmitoylation signal over total wt and mHTT protein and expressed relatively to wtHTT in the control (17Q) group. Mutant HTT was quantified with wtHTT, as it is challenging to resolve full length HTT alleles with small ΔQs with commonly used 3-8% tris-acetate gel.

(**D**) Exponential relationship between HTT global palmitoylation levels and the polyQ tract length (high polyQ) in lymphoblasts.

(**E**) HTT (wt and mutant) palmitoylation levels in HD hPSCs and isogenic controls (Ooi et al., 2019; Xu et al., 2017) with increasing polyQ tract length (18 to 180). Proteins were resolved using 3-8% tris-acetate gels. The white arrowhead indicates an unidentified band only detected with streptavidin. The hPSC parental lines used to generate HD or control hPSC lines are annotated with an asterisk.

(**F**) Exponential relationship between HTT global palmitoylation level and the polyQ tract length (high polyQ) in hPSCs.

Statistical analysis: 1-way ANOVA: (**B**) p=0.027; (**C**) p=0.037. Stars indicate Tukey's multiple comparisons test results. (**D**) Variance explained by polyQ tract length, R^2=0.57. Pearson r=-0.75; p=0.018. (**F**) Variance explained by polyQ tract length, R^2=0.43. Pearson r=-0.65; p=0.15.

We quantified the palmitoylation levels of wt and mHTT separately (**Figure 3.B**) or wt and mHTT together (**Figure 3.C**) and observed that mHTT and global HTT palmitoylation levels were significantly decreased with increased polyQ tract length (1WA: (**B**) p=0.027, Tk: p=0.016 for mHTT (>59Q) vs. wtHTT (17Q) and p=0.057 for mHTT (>59Q) vs. wtHTT (~44Q); (**C**) p=0.037, Tk: p=0.031 for total HTT(>59Q) vs. total HTT (17Q)). The exponential relationship between the global palmitoylation level of HTT (wt and mHTT together) and the polyQ tract length (high polyQ) in each lymphoblastoid line is displayed in **Figure 3.D** and supports a negative linear relationship between the two parameters (correlation, p(two-tailed) =0.018).

Palmitoylation levels were also investigated in isogenic HD human pluripotent stem cells (hPSCs) previously generated (Ooi et al., 2019; Xu et al., 2017) using the IP-ABE

488 assay (**Figure 3.E**). The exponential relationship between the global palmitoylation level
489 of HTT (WT and mHTT together) and the polyQ tract length (high polyQ) in each hPSC
490 line (**Figure 3.F**) suggests a negative linear relationship between palmitoylation and
491 polyQ length without reaching statistical significance (correlation, p(two-tailed) =0.14).

492 Our findings in patient-derived cell lines further validate the impact of the HD
493 mutation on HTT palmitoylation levels and suggest that palmitoylation levels of wt and
494 mHTT decreases with increasing polyQ length.

495 **3.4 ASO-mediated mHTT lowering in the brain of the YAC128 HD mouse model does**
496 **not rescue palmitoylation of HIP14 and HIP14L synaptic substrates**

497 We next wanted to evaluate the impact of mHTT lowering in the CNS on
498 palmitoylation of HTT and HIP14/14L substrates. Five-month-old YAC128 mice received
499 intracerebroventricular (ICV) injection of either PBS (n=6) or an ASO targeting human
500 HTT (HTT-ASO; n=7) (Southwell et al., 2015). Brains were collected 1 month later, and
501 palmitoylation of HTT, SNAP25, PSD95 and GAD65 was measured using the IP-ABE
502 assay (**Figure 4**). As expected, mHTT levels in the whole brain were lowered by
503 approximately 90%, whereas levels of mouse Htt remained unchanged (**Figure 4.A**).

504 We measured a 30% reduction of mHTT palmitoylation compared to mouse Htt
505 (2WA: $p<0.0001$, HD mutation, $p<0.0001$) in the PBS controls (Tk: $p=0.049$) and a 60%
506 reduction in the ASO treated animals (Tk: $p<0.0001$), but the ASO treatment did not
507 change Htt and mHTT palmitoylation levels (**Figure 4.B**). ASO treatment also did not
508 significantly alter the palmitoylation level of SNAP25 (**Figure 4.C**), PSD95 (**Figure 4.D**)

509 and GAD65 (**Figure 4.E**). Taken together, mHTT lowering in the brain of the YAC128

510 mouse did not rescue aberrant palmitoylation of the proteins examined.

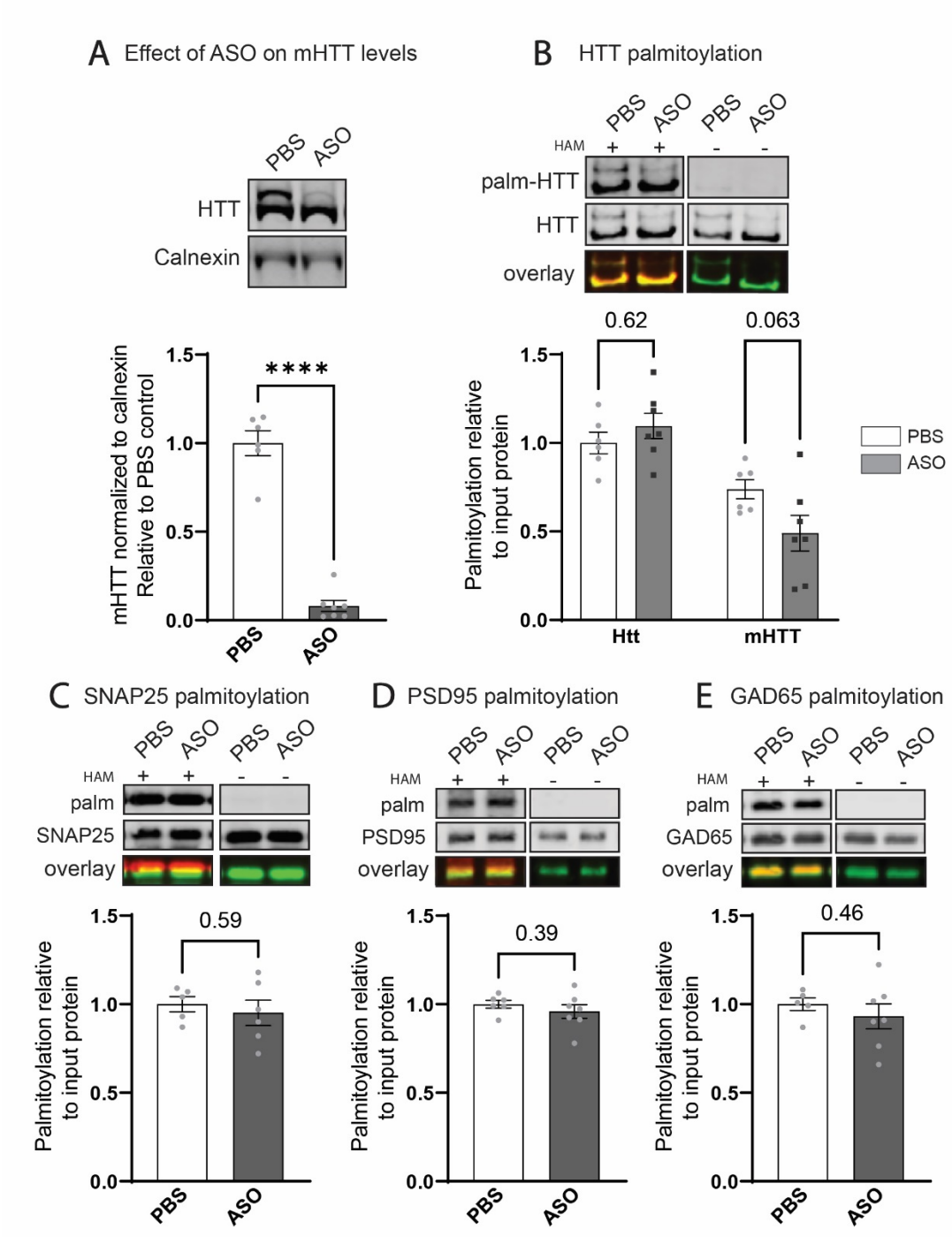

511

512 **<u>Figure 4</u> – ASO-mediated mHTT lowering does not rescue aberrant palmitoylation**

513 **of HIP14/HIP14L synaptic substrates in the brain of the YAC128 mouse model.**

514 Five-month-old YAC128 mice received intracerebroventricular (ICV) injection of either
515 PBS (n=6) or an ASO targeting human HTT (HTT-ASO; n=7), and brains were collected
516 1 month later.

517 (**A**) Protein from brain lysates were separated using 3-8% tris-acetate gradient gel and
518 probed with HTT (MAB2166) and calnexin antibodies. HTT levels were quantified by
519 densitometry and normalized to calnexin, and relative levels of mHTT are shown.

520 Palmitoylation of HTT (**B**), SNAP25 (**C**), PSD95 (**D**) and GAD65 (**E**) was measured using
521 the IP-ABE assay. The palmitoylation signal (HAM+) is shown in the top panels for each
522 protein, and the total protein immunoprecipitated is presented in the panels below. The
523 negative control (HAM-) is displayed on the right of each set of blots. Overlay of both
524 channel (palmitoylated protein in red and total protein in green) are displayed in the
525 bottom panels. In the HTT blots (**B**), the lower band corresponds to mouse Htt, and the
526 upper band to mHTT. The palmitoylation levels were calculated as a ratio of palmitoylation
527 over total protein signal.

528 Statistical analysis: (**B**) 2-way ANOVA: interaction, $p=0.059$; allele, $p<0.0001$, ASO
529 treatment, $p=0.48$. Stars indicate Tukey's multiple comparisons test results between PBS
530 and ASO groups. Student's T-test: (**A**, **C**, **D**, **E**) results are indicated by p-values or stars
531 on the graphs.

532 **3.5. Inhibition of APT increases palmitoylation levels of HTT in COS-7 cells, YAC128**
533 **cortico-striatal primary neurons and HD patient-derived lymphoblasts**

534 Since ASO-mediated mHTT lowering *in vivo* did not rescue the reduced
535 palmitoylation observed in YAC128 brains, we hypothesized that promoting this
536 modification pharmacologically may represent a relevant therapeutic approach for HD.
537 Therefore, our next objective was to assess if HTT palmitoylation levels can be
538 upregulated in various HD models using alternative approaches. To test this, we chose
539 to reduce protein depalmitoylation via the inhibition of the APT enzymes that catalyze
540 thioester hydrolysis of palmitoylated cysteine residues (**Figure 5**). We chose the well
541 characterized and membrane-permeable chiral acyl-β-lactone Palmostatin B (PalmB)
542 (IC_{50} = 5.4 nM) that inhibits the APT1 and APT2 enzymes (Dekker et al., 2010; Vujic et
543 al., 2016). PalmB has also been shown to partially inhibit the activity of FASN, PNPLA6,
544 and ABHD proteins (Lin and Conibear, 2015a).

545 The impact of PalmB treatment on mHTT palmitoylation levels in COS-7 cells
546 transiently expressing N-terminal fragments HTT_{1-548} (N548), HTT_{1-1212} (N1212) or full
547 length HTT_{1-3144} 18Q (wt) or 128Q was assessed by metabolic labelling with palmitic acid
548 alkyne followed by bioorthogonal labelling (click chemistry) (**Figure 5.A**). The PalmB
549 concentration of 15 µM was selected after testing a wide range of concentrations (0, 10,
550 15, 20 and 50 µM) in our experimental models. Palmitoylation levels of N548, N1212 and
551 full length HTT were significantly decreased in the presence of the HD mutation, with a
552 stronger effect for shorter fragments (2WA: HD mutation, $p<0.0001$ for N548 and N1212,
553 and $p=0.0002$ for full length HTT). Treatment of COS-7 cells with 15 µM PalmB for 6h
554 significantly increased the palmitoylation levels of 15Q and 128Q N548, N1212 and full
555 length HTT compared to the respective DMSO controls (2WA: PalmB effect: $p<0.0001$ for
556 N548 and full length HTT, and $p=0.0007$ for N1212). Notably, palmitoylation levels of full
557 length mHTT were restored to those of wtHTT following treatment with PalmB.

558 We next used primary cortico-striatal neuronal cultures from YAC18 and YAC128 mice to
559 evaluate the impact of PalmB treatment on HTT palmitoylation levels (**Figure 5.B**). As
560 expected, the palmitoylation level of mHTT was significantly decreased compared to
561 mouse Htt and wtHTT (2WA: HD mutation, $p<0.0001$). Treatment with PalmB significantly
562 increased human HTT palmitoylation (2WA: PalmB effect, $p=0.032$). In the YAC128
563 neuronal cultures, mouse Htt and mHTT palmitoylation were significantly increased by
564 the PalmB treatment compared to the DMSO control by approximately 20% (Bonferroni's
565 test (Bf): $p=0.041$ and $p=0.028$). In the YAC18 neuronal culture, the effect of PalmB on
566 the palmitoylation levels of mouse Htt and human wtHTT (not distinguishable with our
567 protocol) was weaker (Bf: $p=0.54$).

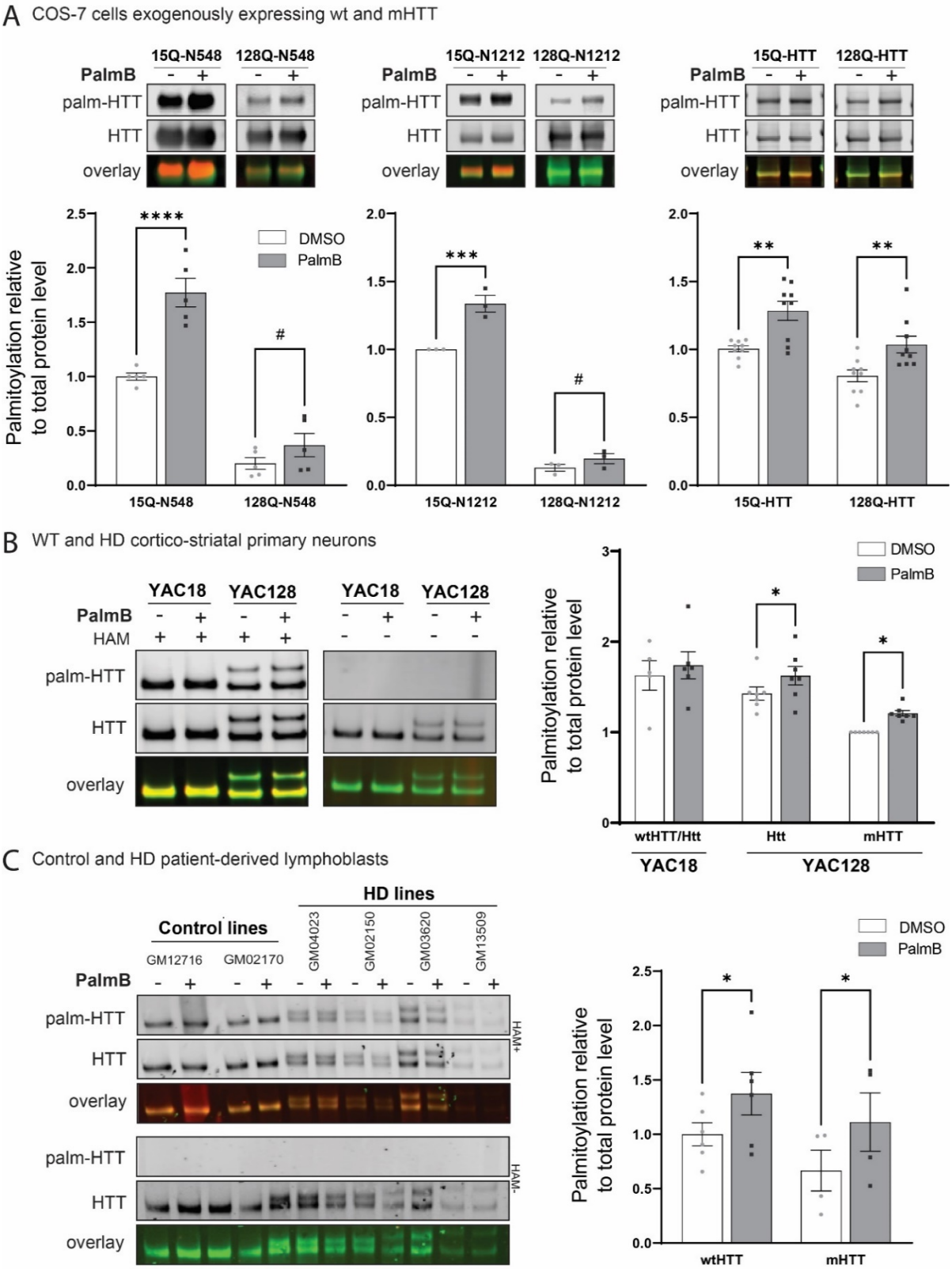

Figure 5 - **Inhibition of APTs with Palmostatin B increases palmitoylation level of HTT in COS-7 cells, YAC128 primary neurons and HD-patient derived lymphoblasts**.

571 (**A**) COS-7 cells were transfected with the N-terminal fragments HTT_{1-548} (N548), HTT_{1-1212} (N1212) and full length wt (15Q) or mutant (128Q) HTT_{1-3144} constructs. Cells were treated with DMSO or 15 µM PalmB for 6h while concurrently labelled with 100 µM alkyne-palmitate. Bio-orthogonal click chemistry of alkyne-palmitate was performed on lysates immunoprecipitated with anti-HTT (MAB2166) antibodies. Palmitoylated and total HTT were detected by immunoblots using streptavidin and anti-HTT (HD46) antibodies, respectively. Overlay of both channel (palm in red and total protein in green) are displayed in the bottom panels. Palmitoylation was calculated as a ratio of palmitoylation signal over total HTT protein and are expressed relative to wtHTT palmitoylation in the DMSO control group.

581 (**B**) YAC18 and YAC128 cortico-striatal primary neurons were treated at DIV10 with DMSO or 15 µM PalmB for 6h. Cell lysates were subjected to the IP-ABE assay to measure palmitoylated HTT. HTT was immunoprecipitated with anti-HTT (MAB2166) antibodies and detected with D7F7 for Htt (mouse) or HTT (human) and streptavidin for palmitoylated protein. HTT palmitoylation level was calculated as a ratio of palmitoylation signal over total HTT protein and expressed relative to mHTT palmitoylation in the DMSO control group.

588 (**C**) Control and HD-patient derived lymphoblastoid lines were treated at with DMSO or 10 µM PalmB for 4h, and lysates were subjected to the IP-ABE assay. HTT was immunoprecipitated with anti-HTT (MAB2166) antibodies and detected with D7F7 for total HTT and streptavidin for palmitoylated HTT. HTT palmitoylation level was calculated as a ratio of palmitoylation signal over total HTT protein and expressed relative to wtHTT palmitoylation level in the DMSO treated control group.

594 Statistical analysis: 2-way ANOVA: (**A**) N548, interaction, $p=0.0042$; HD mutation, $p<0.0001$; PalmB, <0.0001. N1212, interaction, $p=0.0075$; HD mutation, $p<0.0001$; PalmB, $p=0.0007$. Full length HTT, interaction, $p=0.65$; HD mutation, $p=0.0002$; PalmB, $p<0.0001$. (**B**) Interaction, $p=0.86$; HD mutation, $p<0.0001$; PalmB, $p=0.0320$. (**C**) Interaction, $p=0.90$; HD mutation, $p=0.43$; PalmB, $p=0.0071$. Stars indicate Bonferroni's multiple comparisons test results and hashtag t-test results.

600 Finally, we explored the impact of PalmB treatment on HTT palmitoylation in control and HD-patient derived lymphoblasts (**Figure 5.C**). Notably, treatment with PalmB significantly increased HTT palmitoylation in this model (2WA: PalmB effect, $p=0.0071$), rescuing mHTT palmitoylation levels to wtHTT palmitoylation level.

604 Inhibiting the activity of the APT enzymes with PalmB treatment significantly increased full length HTT palmitoylation levels in immortalized cell lines, primary YAC128 neuronal cultures and HD patient-derived cells. Therefore, the impact of the HD mutation

607 on mHTT palmitoylation is reversible and can be modulated using a small molecule APT
608 inhibitor.

609 **3.6. Inhibition of APTs with PalmB treatment reduces mHTT-induced cytotoxicity in**
610 **COS-7 cells and YAC128 primary neurons**

611 Our last objective was to investigate if increasing mHTT palmitoylation levels
612 through APT inhibition would impact mHTT inclusion formation and/or mHTT-induced cell
613 toxicity in an *in vitro* HD model. We measured the impact of PalmB treatment in COS-7
614 cells transfected with mutant 138Q HTT_{1-588}-YFP (138Q-N588-YFP) on the quantity of
615 insoluble mHTT inclusions using a filter retardation assay (**Figure 6**). We confirmed that
616 PalmB treatment increased 138Q-N588-YFP palmitoylation level (by 30%) compared to
617 the DMSO treated control (p=0.029) (**Figure 6.A**), and that the amount of insoluble HTT
618 inclusions were significantly higher following expression of 138Q-N588-YFP compared to
619 17Q-N588-YFP (p<0.0001) (**Figure 6.B**). Treatment with PalmB for 48h significantly
620 decreased the formation of insoluble inclusions by 20-22% (p=0.038 and 0.0065 with HTT
621 or GFP antibodies) (**Figure 6.C**).

622 The impact of APT inhibition on cytotoxicity was measured using the LDH activity
623 assay in COS-7 cells transiently expressing 15Q or 128Q-HTT_{1-3144}. First, we confirmed
624 that the expression of full length 128Q-HTT increased cytotoxicity (relative to
625 untransfected cells) compared to 15Q-HTT (p=0.019) (**Figure 6.D**). Then, we measured
626 the impact of PalmB treatment for 6 or 24h on cytotoxicity in COS-7 expressing 128Q-
627 HTT (**Figure 6.E**). Negative cytotoxicity values correspond to a protective effect of the
628 treatment. Treatment with PalmB for 6 and 24h significantly reduced cytotoxicity in COS-
629 7 cells expressing 128Q-HTT relative to DMSO controls (2WA: PalmB effect, p<0.0001).

630 The effect of PalmB on cytotoxicity compared to the DMSO control was the strongest at
631 a concentration of 30 μM, but was also significant at lower concentrations (Dunnett's test:
632 $p<0.05$).

633 The impact of PalmB treatment on cytotoxicity was also assessed in YAC128 cortico-
634 striatal primary neurons (**Figure 6.F**). Cytotoxicity was significantly reduced by the PalmB
635 treatment compared to neurons treated with DMSO (2WA: PalmB effect, $p=0.0014$). The
636 effect of PalmB against cytotoxicity compared to the DMSO treated control was the
637 strongest with 10 μM and 15 μM after 6 and 24h or treatment, respectively (Dunnett's
638 test: $p=0.048$ and 0.0098).

639 Altogether, the data shows that inhibiting of APTs with PalmB reduces mHTT
640 inclusion levels and mHTT-induced cytotoxicity in COS-7 cells and YAC128 cortico-
641 striatal primary neurons.

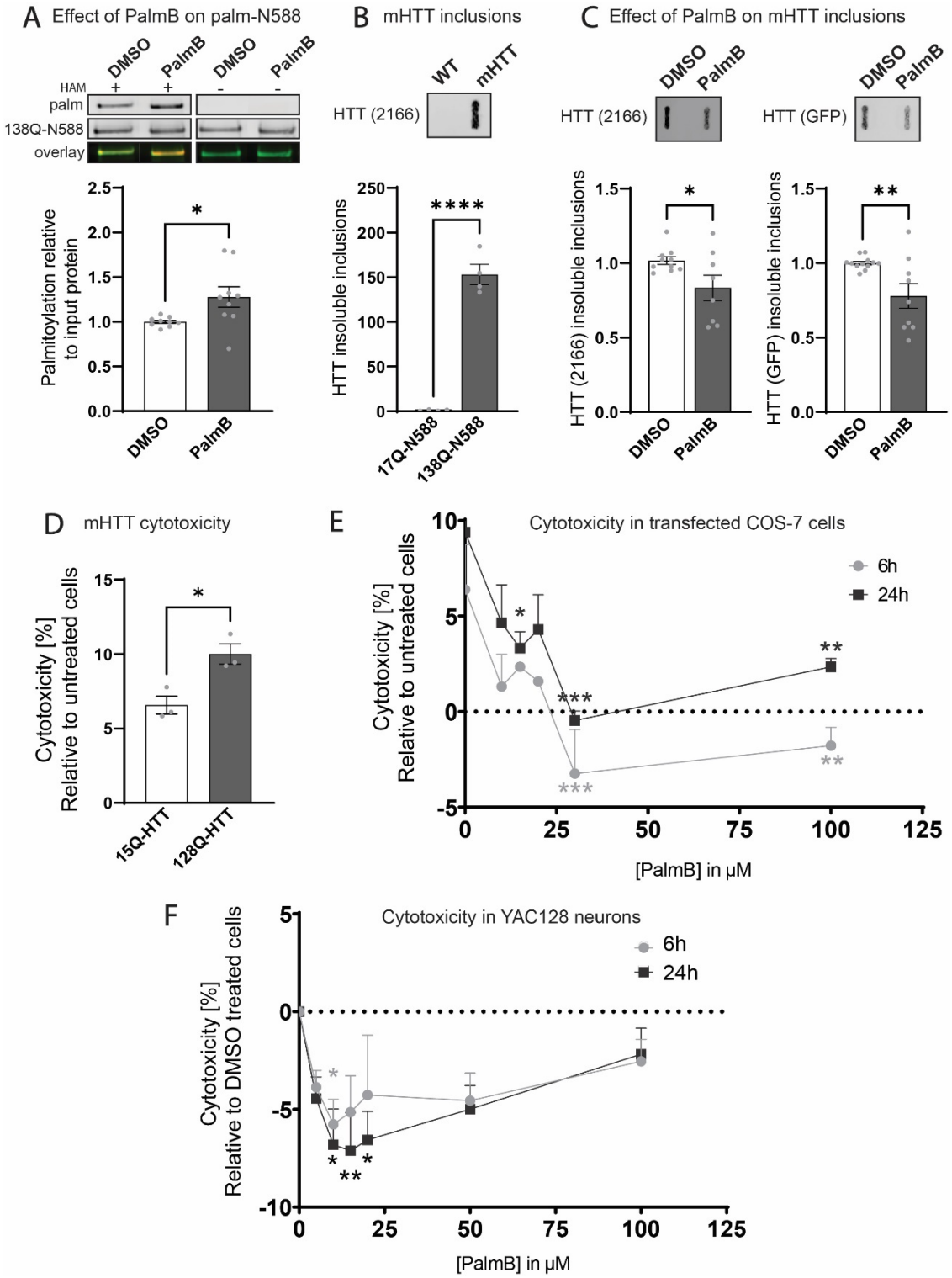

<u>Figure 6</u> - Inhibition of APTs with Palmostatin B reduces mHTT insoluble inclusions in COS-7 cells and mHTT-induced cytotoxicity in COS-7 cells and YAC128 cortico-striatal primary neurons.

646 COS-7 cells were transfected at t=0h with 138Q-HTT$_{1-588}$-YFP (138Q-N588-YFP)
647 construct, treated with 15 µM PalmB at t=24h and 48h post-transfection and harvested at
648 t=72h.

649 (**A**) Cell lysates were subjected to the IP-ABE assay to measure palmitoylated HTT. HTT
650 was immunoprecipitated with anti-GFP antibodies and detected with MAB2166 for HTT
651 and streptavidin for palmitoylated protein. HTT palmitoylation level was calculated as a
652 ratio of palmitoylation signal over total HTT protein and expressed relative to
653 palmitoylation in the DMSO control group.

654 (**B-C**) Insoluble mHTT inclusions were monitored by filter retardation assay and
655 immunodetection with anti-HTT (MAB2166) or GFP antibodies. The amount of
656 aggregates retained on the filter is expressed relative to (**B**) 17Q-N588-YFP or (**C**) to the
657 DMSO treated group.

658 (**D**) Expression of full length 128Q-HTT in COS-7 cells increased cytotoxicity compared
659 to 15Q-HTT expression. COS-7 cells seeded in 96-well pates were transfected with WT
660 (15Q) or mutant (128Q) full length HTT for 24h. LDH activity in conditioned media was
661 measured using the CyQUANT cell proliferation assay. Cytotoxicity (%) is expressed
662 relative to untreated and non-transfected cells.

663 (**E**) Cytotoxicity in COS-7 cells transfected for 24h with full length 128Q-HTT and treated
664 with DMSO or PalmB (InSolution at 10, 15, 20, 30 and 100 µM) for 6 or 24h was assessed
665 using the LDH activity assay (n=3). Cytotoxicity (%) is expressed relative to untreated and
666 non-transfected cells. Negative cytotoxicity values correspond to a protective effect.

667 (**F**) Cytotoxicity in YAC128 cortico-striatal primary neurons at DIV15 treated with DMSO
668 or PalmB (InSolution at 5, 10, 15, 20, 50 and 100 µM) for 6 or 24h, using the LDH activity
669 assay (n=4). Cytotoxicity (%) is expressed relatively to YAC128 neurons treated with
670 DMSO. Negative cytotoxicity corresponds to a protective effect. Negative cytotoxicity
671 values correspond to a protective effect.

672 Statistical analysis: Student's T-test (**A**) p=0.029, (**B**) p<0.0001, (**C**) MAB2166, p=0.038
673 and GFP, p=0.0065. (**D**) p=0.019. 2-way ANOVA: (**E**) Interaction, p=0.90, PalmB effect,
674 p<0.0001, Treatment duration, p=0.0033; (**F**) Interaction, p=0.97; PalmB, p=0.0014;
675 Treatment duration, p=0.29. Stars indicate Dunnett's test results compared to respective
676 DMSO control.

677 **4. Discussion**

678 Targeting the cause of HD, by lowering levels of the toxic mHTT protein, is one of
679 the therapeutic strategies for the treatment of this disease (Caron et al., 2018). This can
680 be achieved by suppressing transcription of *HTT*, degrading the transcript, reducing
681 synthesis of the toxic protein or increasing its degradation in cells. Promising strategies
682 to promote mHTT degradation use mHTT-LC3 linker compounds (Li et al., 2019) or
683 proteolysis-targeting chimera (PROTAC) based approaches (Harding and Tong, 2018).
684 Another approach has been to target specific PTMs of HTT that are dysregulated in
685 presence of the HD mutation in order to promote neuronal survival (Aharony et al., 2015;
686 Bowie et al., 2018; Di Pardo et al., 2012; Ehrnhoefer et al., 2011; Gu et al., 2009; Kratter
687 et al., 2016).

688 The challenge with this strategy lies in the identification of the enzymes that
689 modulate PTMs with a high specificity for HTT. Most kinases, phosphatases or caspases
690 have a large variety of substrates. Developing therapeutically relevant pharmacological
691 modulators of PTMs requires that they be developed within the context of well-
692 characterized PTM-related signaling systems. However, there are still many knowledge
693 gaps regarding the role of PTM dysregulation on mHTT toxicity in HD that need to be
694 addressed to develop effective therapies.

695 A potential PTM candidate is palmitoylation of HTT at cysteine 214, catalyzed by
696 HIP14 (ZDHHC17) and HIP14L (ZDHHC13) (Yanai et al., 2006). Here, we showed that
697 palmitoylation levels of HTT and various HIP14/14L substrates were reproducibly reduced
698 in a variety of HD models, including humanized HD mouse models, HD patient-derived
699 lymphoblast and isogenic hiPSCs (**Figures 1 and 3**). Palmitoylation of HTT was

700 decreased as early as 1 month of age in the HD humanized mouse model and
701 palmitoylation levels were further decreased with aging (**Figure 2**). Lowering mHTT levels
702 in the YAC128 mouse brain was not sufficient to rescue palmitoylation levels of synaptic
703 HIP14/14L substrates (**Figure 4**). Treatment of COS-7 cells, YAC128 cortico-striatal
704 neurons and in HD patient derived lymphoblast with Palm B, a small molecule that targets
705 mainly APTs 1 and 2, normalized palmitoylation of full length mHTT (**Figure 5**). Finally,
706 modulating mHTT palmitoylation was beneficial against mHTT-induced cytotoxicity
707 (**Figure 6**).

708 Our first aim was to investigate how the HD mutation impacts HTT palmitoylation
709 in multiple mouse and human HD models to address model biases and technical
710 limitations previously encountered and to obtain a more accurate representation of
711 palmitoylation dysregulation that may occur in HD patients. The palmitoylation of mHTT
712 was previously shown to be reduced by 50% in COS-7 cells expressing 15Q and 128Q
713 N548 and metabolically labelled with [^{3}H]-palmitate, and by 80% in the YAC128 HD
714 mouse brain compared to wtHTT in the YAC18 brain (a different mouse line than YAC128
715 expressing endogenous mouse 7Q-Htt and human 18Q-HTT) (Yanai et al., 2006)
716 followed by the earliest version of the ABE assay (Drisdel and Green, 2004), which has
717 since been optimized to yield higher sensitivity (Brigidi and Bamji, 2013).

718 A potential confounding factor of using the YAC128 and BACHD mouse models is
719 the presence of two endogenous mouse Htt alleles in addition to the mHTT transgene,
720 which could compensate for the effect of mHTT on HIP14 and HIP14L activity. To take
721 this into consideration, the two humanized HD mouse models, Hu97/18 and Hu128/21,

722 which harbor a mutant and a wtHTT human transgene with no mouse Htt complement,
723 were also used to investigate palmitoylation in a model that more closely models the
724 human condition. In all four mouse models of HD, mHTT palmitoylation was reproducibly
725 decreased compared to littermate control mice and compared to the WT protein within
726 the same mouse (**Figure 1**).

727 To assess HTT palmitoylation in a more physiologically relevant system, we used
728 control and HD patient-derived lymphoblasts. We observed that palmitoylation of HTT is
729 decreased with increasing number of polyQ repeats (**Figure 3.A-D**). This is, to our
730 knowledge, the first demonstration of aberrant palmitoylation of mHTT in a human-derived
731 HD cell model. This supports the finding that decreased palmitoylation of mHTT in the
732 brains of a variety of HD mouse models is not an artifact due to lower affinity of mouse
733 HIP14/14L (or potentially other PATs) for the human huntingtin protein, but a robust
734 biochemical phenotype. Previous studies have looked at palmitoylation dysregulation in
735 HD models with extreme polyQ lengths (>90) rarely seen in the clinic (Huang et al., 2011;
736 Yanai et al., 2006). Our results now suggest that aberrant palmitoylation of HTT occurs
737 within a range of clinically-relevant polyQ-repeat lengths found in HD patients. We also
738 provide the first evidence that mHTT palmitoylation levels are inversely correlated with
739 polyQ repeat length. The data generated in two sets of isogenic control and HD (IsoHD)
740 hPSC lines (**Figure 3.E-F**) suggests that the differences of palmitoylation level are not
741 due to additional factors such as genetic variants beyond the *HTT* gene.

742 Our next objective was to investigate the earliest timepoint at which palmitoylation
743 is altered in the humanized HD mouse model, Hu128/21 (**Figure 2**). We showed that

744 palmitoylation of mHTT was decreased very early in the whole brain (at 1 month), before
745 onset of behavioural and neuropathological HD-like phenotypes (Southwell et al., 2017),
746 making it one of the earliest phenotypes observed in this model. This downregulation of
747 mHTT palmitoylation is maintained at 3, 6 and 12 months in the brain of Hu128/21.
748 Additional studies are required to determine if mHTT is hypo-palmitoylated during
749 embryonic development.

750 We report here for the first time that aging led to a decrease of both wtHTT and
751 mHTT palmitoylation. This suggests that the presence of the HD mutation has the same
752 impact as aging on HTT palmitoylation levels. The combined impact of aging and the HD
753 mutation may be additive in reducing palmitoylation levels. The relationship between
754 palmitoylation levels of proteins in aging have not been extensively investigated (Zamzow
755 et al., 2019).

756 Therapeutics that lower toxic mHTT have shown promise in preclinical studies in
757 HD rodents (Kordasiewicz et al., 2012; Southwell et al., 2018) and are currently being
758 evaluated in clinical trials for HD (NCT04120493, NCT04000594 and NCT03225833). We
759 have previously shown that reducing levels of Htt in *Htt*$^{+/-}$ mice and FVB neurons treated
760 with pan-HTT ASO (~95% HTT knockdown) leads to reduced palmitoylation of HIP14 and
761 HIP14 substrates such as SNAP25 and GluR1 (Huang et al., 2011). However, the impact
762 of lowering mHTT on palmitoylation of HIP14 and HIP14L substrates has not been
763 investigated. Our data from YAC128 animals treated with an ASO against mHTT at 5
764 months of age and assessed at 6 months of age (**Figure 4;** ~90% reduction of mHTT
765 levels in the whole brain) suggests that mHTT lowering for 1 month is not sufficient to

766 rescue palmitoylation alterations in HD. This suggest that specific palmitoylation-targeted
767 therapies may be necessary. Additional studies to investigate the impact of ASO treatment
768 at a younger age, or for a longer duration are needed.

769 Aberrant palmitoylation causes or contributes to a large variety of disorders such
770 as Alzheimer's disease , schizophrenia, mental retardation and Batten Disease
771 (Bhattacharyya et al., 2013; Cho and Park, 2016; Hofmann and Lu, 2014; Ko and Dixon,
772 2018). The concept of developing therapeutically relevant pharmacological modulators of
773 palmitoylation to promote or reduce palmitoylation of specific proteins has been an
774 emerging field over the past years (Chavda et al., 2014; Fraser et al., 2019). In this study,
775 we observed robust reduction of HTT palmitoylation in a variety of HD models. HTT is
776 dynamically palmitoylated by HIP14 and 14L and de-palmitoylated by APTs 1 and 2 (also
777 LYPA1 and 2) (Lin and Conibear, 2015b; Yanai et al., 2006). We have previously shown
778 that increasing mHTT palmitoylation levels *in vitro* by overexpression of HIP14 may be
779 protective (Yanai et al., 2006), but this approach is not easily translatable *in vivo*. Inhibition
780 of APTs with the membrane-permeable chiral acyl-β-lactone PalmB (Davda and Martin,
781 2014; Dekker et al., 2010; Vujic et al., 2016) was shown to increase HTT_{1-548}
782 palmitoylation levels in COS-7 cells (Lin and Conibear, 2015b). Here, we demonstrate
783 that PalmB can be used to promote palmitoylation of full length mHTT in multiple models
784 (**Figure 5**).

785 This study serves as a proof-of-concept that mHTT palmitoylation can be
786 increased, and even normalized to wtHTT levels, using a small molecule. Furthermore,
787 we show that increasing palmitoylation of mHTT exerts beneficial effects on aggregation

788 and cytotoxicity (**Figure 6**). Protective effects of promoting palmitoylation of HTT and
789 other substrates may be mediated by increased mHTT clearance, or reduced proteolytic
790 cleavage of mHTT by caspase 6 (CASP6) at D586. We have indeed recently shown that
791 CASP6 is palmitoylated by HIP14, resulting in CASP6 inactivation (Lontay et al., 2020;
792 Skotte et al., 2017) which would be expected to reduce cleavage and potentially provide
793 beneficial effects.

794 Further studies evaluating the impact of promoting HTT palmitoylation on well
795 characterized HD phenotypes will help elucidate the potential mechanism of action
796 leading to the observed protective effects. PalmB inhibits APT 1 and 2 that depalmitoylate
797 a large variety of protein substrates, and also targets FASN, PNPLA6, and ABHD proteins
798 (Lin and Conibear, 2015a). Testing additional APT inhibitors (Vujic et al., 2016) or
799 developing new candidate small molecules that specifically disrupt the interaction
800 between APTs and HTT or HIP14 will be important for advancing this therapeutic strategy
801 for HD.

802 **Acknowledgments & Funding**

803 The authors would like to thank Mark Wang, Xiaofan Qu and Qingwen Xia for their
804 technical support, Dr. Amirah Ali, Dr. Philip Ly, Hailey Findlay-Black, Jennifer Collins, Dr.
805 Niels Skotte, Dr. Amber Southwell and Stephanie Bortnick for their support on the project.
806 FLL was funded by a Canadian Institutes of Health Research (CIHR) Postdoctoral
807 Fellowship. NSC was funded by the Ripples of Hope Pfizer Trainee Award, a Canadian
808 Institutes for Health Research Postdoctoral Fellowship, and the Huntington Disease
809 Society of America Berman/Topper Family HD Career Development Fellowship. MES
810 was supported by a Vanier Canada Graduate Scholarship and a University of British
811 Columbia 4-Year Graduate Fellowship. MAP is Michael Smith Foundation for Health
812 Research Scholar. Project operational support for MRH provided by a CIHR Foundation
813 grant (FDN-154278) and by the CHDI Foundation.

814 **Conflict of Interest**

815 The authors have no conflict of interest to report.

BIBLIOGRAPHY

Aharony, I., Ehrnhoefer, D.E., Shruster, A., Qiu, X., Franciosi, S., Hayden, M.R., Offen, D., 2015. A Huntingtin-based peptide inhibitor of caspase-6 provides protection from mutant Huntingtin-induced motor and behavioral deficits. Hum Mol Genet 24, 2604–2614. https://doi.org/10.1093/hmg/ddv023

Aiken, C.T., Steffan, J.S., Guerrero, C.M., Khashwji, H., Lukacsovich, T., Simmons, D., Purcell, J.M., Menhaji, K., Zhu, Y.-Z., Green, K., Laferla, F., Huang, L., Thompson, L.M., Marsh, J.L., 2009. Phosphorylation of threonine 3: implications for Huntingtin aggregation and neurotoxicity. J. Biol. Chem. 284, 29427–29436. https://doi.org/10.1074/jbc.M109.013193

Atwal, R.S., Desmond, C.R., Caron, N., Maiuri, T., Xia, J., Sipione, S., Truant, R., 2011. Kinase inhibitors modulate huntingtin cell localization and toxicity. Nat. Chem. Biol. 7, 453–460. https://doi.org/10.1038/nchembio.582

Atwal, R.S., Xia, J., Pinchev, D., Taylor, J., Epand, R.M., Truant, R., 2007. Huntingtin has a membrane association signal that can modulate huntingtin aggregation, nuclear entry and toxicity. Hum. Mol. Genet. 16, 2600–2615. https://doi.org/10.1093/hmg/ddm217

Bhattacharyya, R., Barren, C., Kovacs, D.M., 2013. Palmitoylation of Amyloid Precursor Protein Regulates Amyloidogenic Processing in Lipid Rafts. J Neurosci 33, 11169–11183. https://doi.org/10.1523/JNEUROSCI.4704-12.2013

Bowie, L.E., Maiuri, T., Alpaugh, M., Gabriel, M., Arbez, N., Galleguillos, D., Hung, C.L.K., Patel, S., Xia, J., Hertz, N.T., Ross, C.A., Litchfield, D.W., Sipione, S., Truant, R., 2018. N6-Furfuryladenine is protective in Huntington's disease models by signaling huntingtin phosphorylation. PNAS 115, E7081–E7090. https://doi.org/10.1073/pnas.1801772115

Brigidi, G.S., Bamji, S.X., 2013. Detection of protein palmitoylation in cultured hippocampal neurons by immunoprecipitation and acyl-biotin exchange (ABE). J Vis Exp. https://doi.org/10.3791/50031

Cariulo, C., Azzollini, L., Verani, M., Martufi, P., Boggio, R., Chiki, A., Deguire, S.M., Cherubini, M., Gines, S., Marsh, J.L., Conforti, P., Cattaneo, E., Santimone, I., Squitieri, F., Lashuel, H.A., Petricca, L., Caricasole, A., 2017. Phosphorylation of huntingtin at residue T3 is decreased in Huntington's disease and modulates mutant huntingtin protein conformation. PNAS 114, E10809–E10818. https://doi.org/10.1073/pnas.1705372114

Cariulo, C., Verani, M., Martufi, P., Ingenito, R., Finotto, M., Deguire, S.M., Lavery, D.J., Toledo-Sherman, L., Lee, R., Doherty, E.M., Vogt, T.F., Dominguez, C., Lashuel, H.A., Petricca, L., Caricasole, A., 2020. Ultrasensitive quantitative measurement of huntingtin phosphorylation at residue S13. Biochem. Biophys. Res. Commun. 521, 549–554. https://doi.org/10.1016/j.bbrc.2019.09.097

Caron, N.S., Desmond, C.R., Xia, J., Truant, R., 2013. Polyglutamine domain flexibility mediates the proximity between flanking sequences in huntingtin. Proceedings of the National Academy of Sciences of the United States of America 110, 14610–14615. https://doi.org/10.1073/pnas.1301342110

Caron, N.S., Dorsey, E.R., Hayden, M.R., 2018. Therapeutic approaches to Huntington disease: from the bench to the clinic. Nat Rev Drug Discov 17, 729–750. https://doi.org/10.1038/nrd.2018.133

862 Carroll, J.B., Warby, S.C., Southwell, A.L., Doty, C.N., Greenlee, S., Skotte, N., Hung,
863 G., Bennett, C.F., Freier, S.M., Hayden, M.R., 2011. Potent and selective
864 antisense oligonucleotides targeting single-nucleotide polymorphisms in the
865 Huntington disease gene / allele-specific silencing of mutant huntingtin. Mol Ther
866 19, 2178–2185. https://doi.org/10.1038/mt.2011.201
867 Chavda, B., Arnott, J.A., Planey, S.L., 2014. Targeting protein palmitoylation: selective
868 inhibitors and implications in disease. Expert Opin Drug Discov 9, 1005–1019.
869 https://doi.org/10.1517/17460441.2014.933802
870 Cho, E., Park, M., 2016. Palmitoylation in Alzheimer's disease and other
871 neurodegenerative diseases. Pharmacol. Res. 111, 133–151.
872 https://doi.org/10.1016/j.phrs.2016.06.008
873 Davda, D., Martin, B.R., 2014. Acyl protein thioesterase inhibitors as probes of dynamic
874 S-palmitoylation. Medchemcomm 5, 268–276.
875 https://doi.org/10.1039/C3MD00333G
876 Dekker, F.J., Rocks, O., Vartak, N., Menninger, S., Hedberg, C., Balamurugan, R.,
877 Wetzel, S., Renner, S., Gerauer, M., Schölermann, B., Rusch, M., Kramer, J.W.,
878 Rauh, D., Coates, G.W., Brunsveld, L., Bastiaens, P.I.H., Waldmann, H., 2010.
879 Small-molecule inhibition of APT1 affects Ras localization and signaling. Nat.
880 Chem. Biol. 6, 449–456. https://doi.org/10.1038/nchembio.362
881 Di Pardo, A., Maglione, V., Alpaugh, M., Horkey, M., Atwal, R.S., Sassone, J.,
882 Ciammola, A., Steffan, J.S., Fouad, K., Truant, R., Sipione, S., 2012. Ganglioside
883 GM1 induces phosphorylation of mutant huntingtin and restores normal motor
884 behavior in Huntington disease mice. Proc. Natl. Acad. Sci. U.S.A. 109, 3528–
885 3533. https://doi.org/10.1073/pnas.1114502109
886 Drisdel, R.C., Green, W.N., 2004. Labeling and quantifying sites of protein
887 palmitoylation. BioTechniques 36, 276–285.
888 Ehrnhoefer, D.E., Sutton, L., Hayden, M.R., 2011. Small changes, big impact:
889 posttranslational modifications and function of huntingtin in Huntington disease.
890 Neuroscientist 17, 475–492. https://doi.org/10.1177/1073858410390378
891 Evans, S.J.W., Douglas, I., Rawlins, M.D., Wexler, N.S., Tabrizi, S.J., Smeeth, L., 2013.
892 Prevalence of adult Huntington's disease in the UK based on diagnoses recorded
893 in general practice records. J. Neurol. Neurosurg. Psychiatry 84, 1156–1160.
894 https://doi.org/10.1136/jnnp-2012-304636
895 Fisher, E.R., Hayden, M.R., 2014. Multisource ascertainment of Huntington disease in
896 Canada: prevalence and population at risk. Mov. Disord. 29, 105–114.
897 https://doi.org/10.1002/mds.25717
898 Fraser, N.J., Howie, J., Wypijewski, K.J., Fuller, W., 2019. Therapeutic targeting of
899 protein S-acylation for the treatment of disease. Biochemical Society
900 Transactions 48, 281–290. https://doi.org/10.1042/BST20190707
901 Fukata, Y., Fukata, M., 2010. Protein palmitoylation in neuronal development and
902 synaptic plasticity. Nat. Rev. Neurosci. 11, 161–175.
903 https://doi.org/10.1038/nrn2788
904 Globa, A.K., Bamji, S.X., 2017. Protein palmitoylation in the development and plasticity
905 of neuronal connections. Curr Opin Neurobiol 45, 210–220.
906 https://doi.org/10.1016/j.conb.2017.02.016

907 Graham, R.K., Deng, Y., Slow, E.J., Haigh, B., Bissada, N., Lu, G., Pearson, J.,
908 Shehadeh, J., Bertram, L., Murphy, Z., Warby, S.C., Doty, C.N., Roy, S.,
909 Wellington, C.L., Leavitt, B.R., Raymond, L.A., Nicholson, D.W., Hayden, M.R.,
910 2006. Cleavage at the caspase-6 site is required for neuronal dysfunction and
911 degeneration due to mutant huntingtin. Cell 125, 1179–1191.
912 https://doi.org/10.1016/j.cell.2006.04.026
913 Gray, M., Shirasaki, D.I., Cepeda, C., André, V.M., Wilburn, B., Lu, X.-H., Tao, J.,
914 Yamazaki, I., Li, S.-H., Sun, Y.E., Li, X.-J., Levine, M.S., Yang, X.W., 2008. Full-
915 length human mutant huntingtin with a stable polyglutamine repeat can elicit
916 progressive and selective neuropathogenesis in BACHD mice. J. Neurosci. 28,
917 6182–6195. https://doi.org/10.1523/JNEUROSCI.0857-08.2008
918 Gu, X., Greiner, E.R., Mishra, R., Kodali, R., Osmand, A., Finkbeiner, S., Steffan, J.S.,
919 Thompson, L.M., Wetzel, R., Yang, X.W., 2009. Serines 13 and 16 are critical
920 determinants of full-length human mutant huntingtin induced disease
921 pathogenesis in HD mice. Neuron 64, 828–840.
922 https://doi.org/10.1016/j.neuron.2009.11.020
923 Harding, R.J., Tong, Y., 2018. Proteostasis in Huntington's disease: disease
924 mechanisms and therapeutic opportunities. Acta Pharmacol Sin 39, 754–769.
925 https://doi.org/10.1038/aps.2018.11
926 Hofmann, S., Lu, J.-Y., 2014. Molecular basis of infantile Batten disease: impact of
927 disordered palmitoylated protein degradation on the nervous system (466.1). The
928 FASEB Journal 28, 466.1. https://doi.org/10.1096/fasebj.28.1_supplement.466.1
929 Huang, K., Sanders, S., Singaraja, R., Orban, P., Cijsouw, T., Arstikaitis, P., Yanai, A.,
930 Hayden, M.R., El-Husseini, A., 2009. Neuronal palmitoyl acyl transferases exhibit
931 distinct substrate specificity. FASEB J. 23, 2605–2615.
932 https://doi.org/10.1096/fj.08-127399
933 Huang, K., Sanders, S.S., Kang, R., Carroll, J.B., Sutton, L., Wan, J., Singaraja, R.,
934 Young, F.B., Liu, L., El-Husseini, A., Davis, N.G., Hayden, M.R., 2011. Wild-type
935 HTT modulates the enzymatic activity of the neuronal palmitoyl transferase
936 HIP14. Hum Mol Genet 20, 3356–3365. https://doi.org/10.1093/hmg/ddr242
937 Huang, K., Yanai, A., Kang, R., Arstikaitis, P., Singaraja, R.R., Metzler, M., Mullard, A.,
938 Haigh, B., Gauthier-Campbell, C., Gutekunst, C.-A., Hayden, M.R., El-Husseini,
939 A., 2004. Huntingtin-Interacting Protein HIP14 Is a Palmitoyl Transferase
940 Involved in Palmitoylation and Trafficking of Multiple Neuronal Proteins. Neuron
941 44, 977–986. https://doi.org/10.1016/j.neuron.2004.11.027
942 Hubalkova, P., Ladislav, M., Vyklicky, V., Smejkalova, T., Krausova, B.H., Kysilov, B.,
943 Krusek, J., Naimová, Z., Korinek, M., Chodounska, H., Kudova, E., Cerny, J.,
944 Vyklicky, L., 2021. Palmitoylation Controls NMDA Receptor Function and Steroid
945 Sensitivity. J. Neurosci. 41, 2119–2134.
946 https://doi.org/10.1523/JNEUROSCI.2654-20.2021
947 Humbert, S., Bryson, E.A., Cordelières, F.P., Connors, N.C., Datta, S.R., Finkbeiner, S.,
948 Greenberg, M.E., Saudou, F., 2002. The IGF-1/Akt pathway is neuroprotective in
949 Huntington's disease and involves Huntingtin phosphorylation by Akt. Dev. Cell
950 2, 831–837.
951 Jeong, H., Then, F., Melia, T.J., Mazzulli, J.R., Cui, L., Savas, J.N., Voisine, C.,
952 Paganetti, P., Tanese, N., Hart, A.C., Yamamoto, A., Krainc, D., 2009.

953 Acetylation Targets Mutant Huntingtin to Autophagosomes for Degradation. Cell
954 137, 60–72. https://doi.org/10.1016/j.cell.2009.03.018
955 Kalchman, M.A., Graham, R.K., Xia, G., Koide, H.B., Hodgson, J.G., Graham, K.C.,
956 Goldberg, Y.P., Gietz, R.D., Pickart, C.M., Hayden, M.R., 1996. Huntingtin is
957 ubiquitinated and interacts with a specific ubiquitin-conjugating enzyme. J. Biol.
958 Chem. 271, 19385–19394. https://doi.org/10.1074/jbc.271.32.19385
959 Kalchman, M.A., Koide, H.B., McCutcheon, K., Graham, R.K., Nichol, K., Nishiyama, K.,
960 Kazemi-Esfarjani, P., Lynn, F.C., Wellington, C., Metzler, M., Goldberg, Y.P.,
961 Kanazawa, I., Gietz, R.D., Hayden, M.R., 1997. HIP1 , a human homologue of S.
962 cerevisiae Sla2p , interacts with membrane-associated huntingtin in the brain.
963 Nature Genetics 16, 44–53. https://doi.org/10.1038/ng0597-44
964 Ko, P., Dixon, S.J., 2018. Protein palmitoylation and cancer. EMBO Rep 19.
965 https://doi.org/10.15252/embr.201846666
966 Kordasiewicz, H.B., Stanek, L.M., Wancewicz, E.V., Mazur, C., McAlonis, M.M., Pytel,
967 K.A., Artates, J.W., Weiss, A., Cheng, S.H., Shihabuddin, L.S., Hung, G.,
968 Bennett, C.F., Cleveland, D.W., 2012. Sustained therapeutic reversal of
969 Huntington's disease by transient repression of huntingtin synthesis. Neuron 74,
970 1031–1044. https://doi.org/10.1016/j.neuron.2012.05.009
971 Kratter, I.H., Zahed, H., Lau, A., Tsvetkov, A.S., Daub, A.C., Weiberth, K.F., Gu, X.,
972 Saudou, F., Humbert, S., Yang, X.W., Osmand, A., Steffan, J.S., Masliah, E.,
973 Finkbeiner, S., 2016. Serine 421 regulates mutant huntingtin toxicity and
974 clearance in mice. J Clin Invest 126, 3585–3597.
975 https://doi.org/10.1172/JCI80339
976 Li, Z., Wang, C., Wang, Z., Zhu, C., Li, J., Sha, T., Ma, L., Gao, C., Yang, Y., Sun, Y.,
977 Wang, J., Sun, X., Lu, C., Difiglia, M., Mei, Y., Ding, C., Luo, S., Dang, Y., Ding,
978 Y., Fei, Y., Lu, B., 2019. Allele-selective lowering of mutant HTT protein by HTT-
979 LC3 linker compounds. Nature 575, 203–209. https://doi.org/10.1038/s41586-
980 019-1722-1
981 Lin, D.T.S., Conibear, E., 2015a. ABHD17 proteins are novel protein depalmitoylases
982 that regulate N-Ras palmitate turnover and subcellular localization. eLife 4,
983 e11306. https://doi.org/10.7554/eLife.11306
984 Lin, D.T.S., Conibear, E., 2015b. ABHD17 proteins are novel protein depalmitoylases
985 that regulate N-Ras palmitate turnover and subcellular localization. Elife 4,
986 e11306. https://doi.org/10.7554/eLife.11306
987 Lontay, B., Kiss, A., Virág, L., Tar, K., 2020. How Do Post-Translational Modifications
988 Influence the Pathomechanistic Landscape of Huntington's Disease? A
989 Comprehensive Review. International Journal of Molecular Sciences 21, 4282.
990 https://doi.org/10.3390/ijms21124282
991 Maiuri, T., Mocle, A.J., Hung, C.L., Xia, J., van Roon-Mom, W.M.C., Truant, R., 2017.
992 Huntingtin is a scaffolding protein in the ATM oxidative DNA damage response
993 complex. Hum. Mol. Genet. 26, 395–406. https://doi.org/10.1093/hmg/ddw395
994 Martin, D.D.O., Heit, R.J., Yap, M.C., Davidson, M.W., Hayden, M.R., Berthiaume, L.G.,
995 2014. Identification of a post-translationally myristoylated autophagy-inducing
996 domain released by caspase cleavage of huntingtin. Hum. Mol. Genet. 23, 3166–
997 3179. https://doi.org/10.1093/hmg/ddu027

998 Martin, Dale D. O., Schmidt, M.E., Nguyen, Y.T., Lazic, N., Hayden, M.R., 2018.
999 Identification of a novel caspase cleavage site in huntingtin that regulates mutant
1000 huntingtin clearance. The FASEB Journal 33, 3190–3197.
1001 https://doi.org/10.1096/fj.201701510RRR
1002 Martin, Kay, C., Collins, J.A., Nguyen, Y.T., Slama, R.A., Hayden, M.R., 2018. A human
1003 huntingtin SNP alters post-translational modification and pathogenic proteolysis
1004 of the protein causing Huntington disease. Sci Rep 8, 8096.
1005 https://doi.org/10.1038/s41598-018-25903-w
1006 Matt, L., Kim, K., Chowdhury, D., Hell, J.W., 2019. Role of Palmitoylation of
1007 Postsynaptic Proteins in Promoting Synaptic Plasticity. Front. Mol. Neurosci. 12.
1008 https://doi.org/10.3389/fnmol.2019.00008
1009 Mukai, J., Dhilla, A., Drew, L.J., Stark, K.L., Cao, L., MacDermott, A.B., Karayiorgou, M.,
1010 Gogos, J.A., 2008. Palmitoylation-dependent neurodevelopmental deficits in a
1011 mouse model of 22q11 microdeletion. Nature Neuroscience 11, 1302–1310.
1012 https://doi.org/10.1038/nn.2204
1013 Myers, R.H., 2004. Huntington's disease genetics. NeuroRx 1, 255–262.
1014 https://doi.org/10.1602/neurorx.1.2.255
1015 Ochaba, J., Lukacsovich, T., Csikos, G., Zheng, S., Margulis, J., Salazar, L., Mao, K.,
1016 Lau, A.L., Yeung, S.Y., Humbert, S., Saudou, F., Klionsky, D.J., Finkbeiner, S.,
1017 Zeitlin, S.O., Marsh, J.L., Housman, D.E., Thompson, L.M., Steffan, J.S., 2014.
1018 Potential function for the Huntingtin protein as a scaffold for selective autophagy.
1019 Proc. Natl. Acad. Sci. U.S.A. 111, 16889–16894.
1020 https://doi.org/10.1073/pnas.1420103111
1021 Ooi, J., Langley, S.R., Xu, X., Utami, K.H., Sim, B., Huang, Y., Harmston, N.P., Tay,
1022 Y.L., Ziaei, A., Zeng, R., Low, D., Aminkeng, F., Sobota, R.M., Ginhoux, F.,
1023 Petretto, E., Pouladi, M.A., 2019. Unbiased Profiling of Isogenic Huntington
1024 Disease hPSC-Derived CNS and Peripheral Cells Reveals Strong Cell-Type
1025 Specificity of CAG Length Effects. Cell Rep 26, 2494-2508.e7.
1026 https://doi.org/10.1016/j.celrep.2019.02.008
1027 Sanders, S.S., Hou, J., Sutton, L.M., Garside, V.C., Mui, K.K.N., Singaraja, R.R.,
1028 Hayden, M.R., Hoodless, P.A., 2015a. Huntingtin interacting proteins 14 and 14-
1029 like are required for chorioallantoic fusion during early placental development.
1030 Developmental Biology 397, 257–266.
1031 https://doi.org/10.1016/j.ydbio.2014.11.018
1032 Sanders, S.S., Martin, D.D.O., Butland, S.L., Lavallée-Adam, M., Calzolari, D., Kay, C.,
1033 Iii, J.R.Y., Hayden, M.R., 2015b. Curation of the Mammalian Palmitoylome
1034 Indicates a Pivotal Role for Palmitoylation in Diseases and Disorders of the
1035 Nervous System and Cancers. PLOS Computational Biology 11, e1004405.
1036 https://doi.org/10.1371/journal.pcbi.1004405
1037 Sanders, S.S., Parsons, M.P., Mui, K.K.N., Southwell, A.L., Franciosi, S., Cheung, D.,
1038 Waltl, S., Raymond, L.A., Hayden, M.R., 2016. Sudden death due to paralysis
1039 and synaptic and behavioral deficits when Hip14/Zdhhc17 is deleted in adult
1040 mice. BMC Biol. 14, 108. https://doi.org/10.1186/s12915-016-0333-7
1041 Saudou, F., Humbert, S., 2016. The Biology of Huntingtin. Neuron 89, 910–926.
1042 https://doi.org/10.1016/j.neuron.2016.02.003

1043 Schilling, B., Gafni, J., Torcassi, C., Cong, X., Row, R.H., LaFevre-Bernt, M.A., Cusack,
1044 M.P., Ratovitski, T., Hirschhorn, R., Ross, C.A., Gibson, B.W., Ellerby, L.M.,
1045 2006. Huntingtin phosphorylation sites mapped by mass spectrometry.
1046 Modulation of cleavage and toxicity. J. Biol. Chem. 281, 23686–23697.
1047 https://doi.org/10.1074/jbc.M513507200
1048 Schmidt, M.E., Caron, N.S., Aly, A.E., Lemarié, F.L., Dal Cengio, L., Ko, Y., Lazic, N.,
1049 Anderson, L., Nguyen, B., Raymond, L.A., Hayden, M.R., 2020. DAPK1
1050 Promotes Extrasynaptic GluN2B Phosphorylation and Striatal Spine Instability in
1051 the YAC128 Mouse Model of Huntington Disease. Front. Cell. Neurosci. 14.
1052 https://doi.org/10.3389/fncel.2020.590569
1053 Singaraja, R.R., Huang, K., Sanders, S.S., Milnerwood, A.J., Hines, R., Lerch, J.P.,
1054 Franciosi, S., Drisdel, R.C., Vaid, K., Young, F.B., Doty, C., Wan, J., Bissada, N.,
1055 Henkelman, R.M., Green, W.N., Davis, N.G., Raymond, L.A., Hayden, M.R.,
1056 2011. Altered palmitoylation and neuropathological deficits in mice lacking
1057 HIP14. Hum. Mol. Genet. 20, 3899–3909. https://doi.org/10.1093/hmg/ddr308
1058 Skotte, N.H., Sanders, S.S., Singaraja, R.R., Ehrnhoefer, D.E., Vaid, K., Qiu, X.,
1059 Kannan, S., Verma, C., Hayden, M.R., 2017. Palmitoylation of caspase-6 by
1060 HIP14 regulates its activation. Cell Death & Differentiation 24, 433–444.
1061 https://doi.org/10.1038/cdd.2016.139
1062 Slow, E.J., van Raamsdonk, J., Rogers, D., Coleman, S.H., Graham, R.K., Deng, Y.,
1063 Oh, R., Bissada, N., Hossain, S.M., Yang, Y.-Z., Li, X.-J., Simpson, E.M.,
1064 Gutekunst, C.-A., Leavitt, B.R., Hayden, M.R., 2003. Selective striatal neuronal
1065 loss in a YAC128 mouse model of Huntington disease. Hum Mol Genet 12,
1066 1555–1567. https://doi.org/10.1093/hmg/ddg169
1067 Smotrys, J.E., Linder, M.E., 2004. Palmitoylation of Intracellular Signaling Proteins:
1068 Regulation and Function. Annual Review of Biochemistry 73, 559–587.
1069 https://doi.org/10.1146/annurev.biochem.73.011303.073954
1070 Southwell, A.L., Kordasiewicz, H.B., Langbehn, D., Skotte, N.H., Parsons, M.P.,
1071 Villanueva, E.B., Caron, N.S., Østergaard, M.E., Anderson, L.M., Xie, Y., Cengio,
1072 L.D., Findlay-Black, H., Doty, C.N., Fitsimmons, B., Swayze, E.E., Seth, P.P.,
1073 Raymond, L.A., Frank Bennett, C., Hayden, M.R., 2018. Huntingtin suppression
1074 restores cognitive function in a mouse model of Huntington's disease. Sci Transl
1075 Med 10. https://doi.org/10.1126/scitranslmed.aar3959
1076 Southwell, A.L., Skotte, N.H., Villanueva, E.B., Østergaard, M.E., Gu, X., Kordasiewicz,
1077 H.B., Kay, C., Cheung, D., Xie, Y., Waltl, S., Dal Cengio, L., Findlay-Black, H.,
1078 Doty, C.N., Petoukhov, E., Iworima, D., Slama, R., Ooi, J., Pouladi, M.A., Yang,
1079 X.W., Swayze, E.E., Seth, P.P., Hayden, M.R., 2017. A novel humanized mouse
1080 model of Huntington disease for preclinical development of therapeutics targeting
1081 mutant huntingtin alleles. Hum. Mol. Genet. 26, 1115–1132.
1082 https://doi.org/10.1093/hmg/ddx021
1083 Southwell, A.L., Smith, S.E.P., Davis, T.R., Caron, N.S., Villanueva, E.B., Xie, Y.,
1084 Collins, J.A., Ye, M.L., Sturrock, A., Leavitt, B.R., Schrum, A.G., Hayden, M.R.,
1085 2015. Ultrasensitive measurement of huntingtin protein in cerebrospinal fluid
1086 demonstrates increase with Huntington disease stage and decrease following
1087 brain huntingtin suppression. Sci Rep 5, 12166.
1088 https://doi.org/10.1038/srep12166

1089 Southwell, A.L., Warby, S.C., Carroll, J.B., Doty, C.N., Skotte, N.H., Zhang, W.,
1090 Villanueva, E.B., Kovalik, V., Xie, Y., Pouladi, M.A., Collins, J.A., Yang, X.W.,
1091 Franciosi, S., Hayden, M.R., 2013. A fully humanized transgenic mouse model of
1092 Huntington disease. Hum. Mol. Genet. 22, 18–34.
1093 https://doi.org/10.1093/hmg/dds397
1094 Steffan, J.S., Agrawal, N., Pallos, J., Rockabrand, E., Trotman, L.C., Slepko, N., Illes,
1095 K., Lukacsovich, T., Zhu, Y.-Z., Cattaneo, E., Pandolfi, P.P., Thompson, L.M.,
1096 Marsh, J.L., 2004. SUMO modification of Huntingtin and Huntington's disease
1097 pathology. Science 304, 100–104. https://doi.org/10.1126/science.1092194
1098 Sutton, L.M., Sanders, S.S., Butland, S.L., Singaraja, R.R., Franciosi, S., Southwell,
1099 A.L., Doty, C.N., Schmidt, M.E., Mui, K.K.N., Kovalik, V., Young, F.B., Zhang, W.,
1100 Hayden, M.R., 2013. Hip14l-deficient mice develop neuropathological and
1101 behavioural features of Huntington disease. Hum. Mol. Genet. 22, 452–465.
1102 https://doi.org/10.1093/hmg/dds441
1103 Vujic, I., Sanlorenzo, M., Esteve-Puig, R., Vujic, M., Kwong, A., Tsumura, A., Murphy,
1104 R., Moy, A., Posch, C., Monshi, B., Rappersberger, K., Ortiz-Urda, S., 2016. Acyl
1105 protein thioesterase 1 and 2 (APT-1, APT-2) inhibitors palmostatin B, ML348 and
1106 ML349 have different effects on NRAS mutant melanoma cells. Oncotarget 7,
1107 7297–7306. https://doi.org/10.18632/oncotarget.6907
1108 Wanker, E.E., Scherzinger, E., Heiser, V., Sittler, A., Eickhoff, H., Lehrach, H., 1999.
1109 Membrane filter assay for detection of amyloid-like polyglutamine-containing
1110 protein aggregates. Meth. Enzymol. 309, 375–386.
1111 Warby, S.C., Chan, E.Y., Metzler, M., Gan, L., Singaraja, R.R., Crocker, S.F.,
1112 Robertson, H.A., Hayden, M.R., 2005. Huntingtin phosphorylation on serine 421
1113 is significantly reduced in the striatum and by polyglutamine expansion in vivo.
1114 Hum Mol Genet 14, 1569–1577. https://doi.org/10.1093/hmg/ddi165
1115 Xu, X., Ng, B., Sim, B., Radulescu, C.I., Yusof, N.A.B.M., Goh, W.I., Lin, S., Lim, J.S.Y.,
1116 Cha, Y., Kusko, R., Kay, C., Ratovitski, T., Ross, C., Hayden, M.R., Wright, G.,
1117 Pouladi, M.A., 2020. pS421 huntingtin modulates mitochondrial phenotypes and
1118 confers neuroprotection in an HD hiPSC model. Cell Death & Disease 11, 1–12.
1119 https://doi.org/10.1038/s41419-020-02983-z
1120 Xu, X., Tay, Y., Sim, B., Yoon, S.-I., Huang, Y., Ooi, J., Utami, K.H., Ziaei, A., Ng, B.,
1121 Radulescu, C., Low, D., Ng, A.Y.J., Loh, M., Venkatesh, B., Ginhoux, F.,
1122 Augustine, G.J., Pouladi, M.A., 2017. Reversal of Phenotypic Abnormalities by
1123 CRISPR/Cas9-Mediated Gene Correction in Huntington Disease Patient-Derived
1124 Induced Pluripotent Stem Cells. Stem Cell Reports 8, 619–633.
1125 https://doi.org/10.1016/j.stemcr.2017.01.022
1126 Yanai, A., Huang, K., Kang, R., Singaraja, R.R., Arstikaitis, P., Gan, L., Orban, P.C.,
1127 Mullard, A., Cowan, C.M., Raymond, L.A., Drisdel, R.C., Green, W.N.,
1128 Ravikumar, B., Rubinsztein, D.C., El-Husseini, A., Hayden, M.R., 2006.
1129 Palmitoylation of huntingtin by HIP14 is essential for its trafficking and function.
1130 Nat. Neurosci. 9, 824–831. https://doi.org/10.1038/nn1702
1131 Yap, M.C., Kostiuk, M.A., Martin, D.D.O., Perinpanayagam, M.A., Hak, P.G., Siddam,
1132 A., Majjigapu, J.R., Rajaiah, G., Keller, B.O., Prescher, J.A., Wu, P., Bertozzi,
1133 C.R., Falck, J.R., Berthiaume, L.G., 2010. Rapid and selective detection of fatty

1134 acylated proteins using omega-alkynyl-fatty acids and click chemistry. J. Lipid
1135 Res. 51, 1566–1580. https://doi.org/10.1194/jlr.D002790
1136 Zamzow, D.R., Elias, V., Acosta, V.A., Escobedo, E., Magnusson, K.R., 2019. Higher
1137 Levels of Protein Palmitoylation in the Frontal Cortex across Aging Were
1138 Associated with Reference Memory and Executive Function Declines. eNeuro 6.
1139 https://doi.org/10.1523/ENEURO.0310-18.2019
1140

1141 **Table 1 – List of reagents and chemicals used and application**

1142

	Reagent	Company	Catalogue #
Cell Culture Medium	DMEM without methionine and cystine	ThermoFisher Scientific	21013024
	DMEM/F12	ThermoFisher Scientific	11320033
	Dulbecco's Modified Eagle (DMEM)	ThermoFisher Scientific	11960044
	Neurobasal (NB)	ThermoFisher Scientific	21103049
	RPMI 1640	ThermoFisher Scientific	11875093
	mTeSR™1	STEMCELL Technologies	05850
Cell Culture Reagents	APT1 Inhibitor, palmostatin B	MilliporeSigma	178501
	B27 supplement	ThermoFisher Scientific	17504044
	Corning™ Matrigel™ hESC-Qualified Matrix	Fisher Scientific	354277
	Charcoal stripped FBS	ThermoFisher Scientific	12676029
	Dimethyl sulfoxide (DMSO)	MilliporeSigma	D2650
	DNase I, RNase-free	ThermoFisher Scientific	EN0525
	Fetal Bovine Serum	ThermoFisher Scientific	12483020
	GlutaMAX	ThermoFisher Scientific	35050061
	Hank's balanced salt solution (HBSS) (10X)	ThermoFisher Scientific	14060040
	InSolution™ APT1 Inhibitor, palmostatin B	MilliporeSigma	508738
	Nunc™ EasYFlask™ 25cm^2	ThermoFisher Scientific	156367
	Penicillin-Streptomycin (10,000 U/mL)	ThermoFisher Scientific	15140122
	Phosphate-buffered saline (PBS) (10X)	ThermoFisher Scientific	70011044
	Poly-D-lysine hydrobromide	MilliporeSigma	P7886
	ReLeSR™	STEMCELL Technologies	05872
	Sodium pyruvate	ThermoFisher Scientific	11360070
	Trypsin-EDTA (0.25%), phenol red	ThermoFisher Scientific	25200056
	Trypsin-EDTA (0.05%), phenol red	ThermoFisher Scientific	25300
	X-tremeGENE™ 9 DNA Reagent	MilliporeSigma	6365809001
	6-well, Nunclon delta surface plates	ThermoFisher Scientific	140685
	96-Well, Nunclon Delta-Treated plate	ThermoFisher Scientific	167425
Palmitoylation Assays	Biotin Azide	ThermoFisher Scientific	B10184
	Click Tag™ Palmitic Acid Alkyne	Cayman Chemical	13266
	EZ-Link BMCC-Biotin	ThermoFisher Scientific	21900
	Hydroxylamine hydrochloride	MilliporeSigma	255580
	N-ethylmaleimide (NEM)	MilliporeSigma	E3876
	Triton X-100	MilliporeSigma	T9284
	Tris(benzyltriazolylmethyl)amine (TBTA)	MilliporeSigma	678937
	Tris-carboxyethylphosphine (TCEP)	MilliporeSigma	C4706
	CYQUANT LDH cytotoxicity assay kit	ThermoFisher Scientific	C20303

	Benzonase® Nuclease	MilliporeSigma	E1014-25KU
	Cellulose acetate (OE66) membrane	MilliporeSigma	WHA10404180
Immunoblotting	Protran WB membranes, nitrocellulose	MilliporeSigma	GE10600000
	Dithiothreitol (DTT)	MilliporeSigma	3483-12-3
	Dynabeads™ Protein G	ThermoFisher Scientific	10003D
	Gel Cassettes, mini, 1.5 mm	ThermoFisher Scientific	NC2015
	NuPAGE LDS Sample Buffer (4X)	ThermoFisher Scientific	NP0007
	Invitrogen UltraPure TEMED	ThermoFisher Scientific	15524010
	NuPAGE Novex 3-8% Tris-Acetate gels	ThermoFisher Scientific	EA0375
	Protein Assay Reagent A	Bio-Rad	5000113
	Protein Assay Reagent B	Bio-Rad	5000114
	PureProteome magnetic beads	MilliporeSigma	LSKMAGAG02
	Roche complete Protease Inhibitor Cocktail	MilliporeSigma	11836145001
	Sodium dodecyl sulfate (SDS)	ThermoFisher Scientific	BP166-500
	2% Bis Solution	Bio-Rad	1610142
	30% Acrylamide/Bis Solution, 29:1	Bio-Rad	1610156
	40% Acrylamide Solution	Bio-Rad	1610140

1143

1144 **<u>Table 2</u> – List of antibodies used and application**

Target (clone)	Species	Type	Supplier	Catalogue AB Registry Reference	Application	Dilution	Volume*
HTT (1HU-4C8)	Mouse	Monoclonal	Sigma-Aldrich	MAB2166 AB_2123255	WB	1:1,000	-
					IP	-	2 µL
HTT (D7F7)	Rabbit	Monoclonal	Cell Signaling Technology	5656 AB_10827977	WB	1:1,000	-
HTT (BKP1/HD46)	Rabbit	Polyclonal	in-house	(Kalchman et al., 1997)	IP	-	2 µL
					WB	1:400	-
HTT	Rabbit	Polyclonal	Sigma-Aldrich	H7540 AB_1840946	WB	1:1,000	-
					IP	-	2 µL
Streptavidin	-	Conjugated to AF-680	Invitrogen	S-32358	WB	1:5,000	-
PSD95 (7E3-1B8)	Mouse	Monoclonal	Invitrogen	MA1-046 AB_2092361	WB	1:1,000	-
PSD95	Rabbit	Polyclonal	in-house	-	IP	-	5 µL
GAD65	Rabbit	Polyclonal	Sigma-Aldrich	ABN101	WB	1:1,000	-
	Mouse	Monoclonal	DSHB	GAD-6 AB_2314499	IP	-	3 µL
SNAP25	Rabbit	Polyclonal	Synaptic Systems	111-002 AB_887790	WB	1:1,000	-
SNAP25 (SMI 81)	Mouse	Monoclonal	BioLegend	836303 AB_2715864	IP	-	3 µL
GFP	Rabbit	Polyclonal	Eusera	EU2	WB	1:5,000	-
					IP	-	0.75 µL
Mouse IgM (µ chain specific)	goat	-	Rockland Immuno-chemicals	92632210	WB (secondary)	1:5,000	-
Rabbit IgG	goat	-		926-32211	WB (secondary)	1:5,000	-

1145 *Volume of antibodies used for 20 µL of Dynabeads and 200 µg – 1 mg proteins

1146 **Table 3 – HD mouse lines used for palmitoylation assays**

Mouse model	Line	Reference	Promoter	Transgene product	CAG repeat length	Endogenous product
YAC128	53	(Slow et al., 2003)	Human HTT promoter and RE (24 kb upstream, 117 kb downstream)	full length human mHTT	128	2 copies of 7Q Htt
YAC18	60			2 copies of full length human wtHTT	18	2 copies of 7QnHtt
YAC128	55			2 copies of full length human mHTT	128	2 copies of 7Q Htt
BACHD	LA	(Gray et al., 2008)	Human HTT promoter and RE (20 kb upstream, 50 kb downstream)	full length human mHTT	97	2 copies of 7Q Htt
Hu18/18	KLAY	(Southwell et al., 2013)	Human HTT promoter and RE (20 kb upstream, 50 kb downstream)	full length human wtHTT	18	-
Hu97/18	KLAY			full length human WT and mHTT	97/18	-
Hu21/21	KT53	(Southwell et al., 2017)	Human HTT promoter and RE (24 kb upstream, 117 kb downstream)	full length human wtHTT	21	-
Hu128/21	KT53			full length human wt and mHTT	128/21	-

1147

1148

1149 **Table 4 – Lymphoblastoid cell lines from Coriell Biorepositories**

Catalog ID	Haplotype U/L	Status	Race	Age (years)	Sex	Family	CAG Lower	CAG Upper
GM07029		Control	Caucasian	47	Male	N/a	15	17
GM12716		Control		N/a	Male	1358	15	19
GM02160		Control		21	Male	109	16	17
GM02170		Control		22	Female	111	17	17
GM03863		Control		24	Female	268	17	17
GM03867	N/a	HD	Caucasian	26	Female	268	21	43
GM04023	C/A2	HD		28	Female	587	18	44
GM02176	A1/C	HD		26	Male	110	18	44
GM02150	A2/C	HD		26	Female	108	18	45
GM03620	A1/C	HD		29	Female	110	18	59
GM04724	A3/C	HD		19	Female	691	15	67
GM13509	A3/C	HD		N/a	Female	2706	15	66
GM04282	A3/A4	HD		20	Male	690	17	71

1150

1151

1152

1153 **<u>Table 5</u> – Isogenic HD patient-derived hiPSCs lines**

Cell type	Line	Reference	CAG repeat length
iPSCs	Parental control line (H9)	(Ooi et al., 2019)	30
	IsoHD lines		45
			65
			81
	Parental HD line (CAG180)	(Xu et al., 2017)	180
	Corrected line (HD-C#2)		18

1154